Circulation, Renewal, and Modification of Antarctic Mode and Intermediate Water

Article *in* Journal of Physical Oceanography · April 2001

DOI: 10.1175/1520-0485(2001)031<1005:CRAMOA>2.0.CO;2

2 authors:

Bernadette Sloyan
The Commonwealth Scientific and Industrial …
67 PUBLICATIONS **1,565** CITATIONS
SEE PROFILE

Stephen R. Rintoul
The Commonwealth Scientific and Industrial …
161 PUBLICATIONS **7,542** CITATIONS
SEE PROFILE

Circulation, Renewal, and Modification of Antarctic Mode and Intermediate Water*

BERNADETTE M. SLOYAN+

Alfred Wegener Institute for Polar and Marine Research, Bremerhaven, Germany

STEPHEN R. RINTOUL

Antarctic CRC, University of Tasmania, and CSIRO Division of Marine Research, Hobart, Australia

(Manuscript received 18 October 1999, in final form 10 July 2000)

ABSTRACT

Nine hydrographic sections are combined in an inverse box model of the Southern Ocean south of ~12°S. The inverse model has two novel features: the inclusion of independent diapycnal flux unknowns for each property and the explicit inclusion of air–sea fluxes (heat, freshwater, and momentum) and the water mass transformation they drive. Transformation of 34×10^6 m^3 s^{-1} of Antarctic Surface Water by air–sea buoyancy fluxes, and cooling and freshening where Subantarctic Mode Water outcrops, renews cold, fresh Antarctic Intermediate Water of the southeast Pacific and southwest Atlantic. Relatively cold, fresh mode and intermediate water enter the subtropical gyres, are modified by air–sea fluxes and interior mixing, and return poleward as warmer, saltier mode and intermediate water. While the zonally integrated meridional transport in these layers is small, the gross exchange is approximately 80×10^6 m^3 s^{-1}.

The air–sea transformation of Antarctic surface water to intermediate water is compensated in the Southern Ocean by an interior diapycnal flux of 32×10^6 m^3 s^{-1} of intermediate water to upper deep water. The small property differences between slightly warmer, saltier intermediate water and cold, fresh Antarctic Surface Water results in a poleward transfer of heat and salt across the Polar Front zone.

Mode and intermediate water are crucial participants in the North Atlantic Deep Water overturning and Indonesian Throughflow circulation cells. The North Atlantic Deep Water overturning is closed by cold, fresh intermediate water that is modified to warm, salty varieties by air–sea fluxes and interior mixing in the Atlantic and southwest Indian Oceans. The Indonesian Throughflow is part of a circum-Australia circulation. In the Indian Ocean, surface water is converted to denser thermocline and mode water by air–sea fluxes and interior mixing, excess mode water flows eastward south of Australia, and air–sea fluxes convert mode water to thermocline water in the Pacific.

1. Introduction

The mid-depth salinity minimum layer characterizing Antarctic Intermediate Water (AAIW) is one of the most prominent features of the Southern Hemisphere oceans. The low-salinity core extends northwards from the Antarctic Polar Front (APF) zone at a depth of about 1000 m beneath the subtropical gyres in each basin. In the Atlantic, the AAIW core can be traced across the equator and into the North Atlantic (Wüst 1935), where it supplies a large fraction of the northward flow required to balance the export of North Atlantic Deep Water (Schmitz and Richardson 1991). In the subantarctic zone, a thermostad usually overlies the salinity minimum. The thermostad is associated with Subantarctic Mode Water (SAMW), which is formed by deep mixing in winter on the equatorward side of the Antarctic Circumpolar Current (ACC) (McCartney 1977). Deep winter mixing imprints SAMW with its characteristic properties: low potential vorticity and high oxygen.

Early investigators (Deacon 1937) suggested that circumpolar formation of AAIW resulted from the sinking of Antarctic Surface Water (AASW) below the Subantarctic Front (SAF). This circumpolar formation mechanism is now essentially replaced by theories that suggest renewal of AAIW occurs in specific regions of the Southern Ocean—the southeast Pacific and southwest Atlantic sectors (McCartney 1977; Georgi 1979; Molinelli 1981; Piola and Georgi 1982; Piola and Gordon 1989). Although there appears to be consensus that AAIW is renewed in the southeast Pacific and southwest

* Alfred Wegener Institute for Polar and Marine Research Contribution Number 1783.

+ Current affiliation: NOAA/Pacific Marine Environmental Laboratory/Ocean Climate Research Division, Seattle, Washington.

Corresponding author address: Dr. Bernadette Sloyan, NOAA/PMEL/OCRD, Bldg. 3, 7600 Sand Point Way NE, Seattle, WA 98115-6349.
E-mail: sloyan@pmel.noaa.gov

Atlantic, there is still considerable debate over the mixing mechanisms involved.

McCartney (1977) suggests that the formation of AAIW is explicitly linked to Subantarctic Mode Water. He notes that SAMW and AAIW in the southeast Pacific and southwest Atlantic regions have identical *T*–*S* properties. SAMW is progressively cooled and freshened along its circumpolar path by consecutive deep winter mixing events, resulting in the coldest freshest SAMW in the southeast Pacific and southwest Atlantic, and thus AAIW (McCartney 1977). Molinelli (1981), on the other hand, suggests that AAIW is formed by isopycnal exchange across the Polar Front. Although isopycnal mixing could be a circumpolar source of AAIW, Molinelli (1981) suggests significant inputs near Kerguelen Island (80°E) and in the southeast Pacific. Georgi (1979) and Piola and Georgi (1982) identify two separate pools of AAIW—in the southeast Pacific and southwest Atlantic. They support McCartney's (1977) AAIW renewal mechanism in the southeast Pacific, but in the southwest Atlantic suggest that AAIW is produced near the Polar Front as proposed by Molinelli (1981). Piola and Gordon (1989) show a connection between AAIW in Drake Passage and in the southwest Atlantic. They find that the modification of Drake Passage AAIW to colder, fresher AAIW in the southwest Atlantic can be explained by a combination of further deep winter mixing and exchange of Antarctic surface water across the Polar Front, essentially combining the formation theories of McCartney (1977) and Molinelli (1981).

SAMW and AAIW formed in the Southern Ocean are transported eastward with the ACC and northward into the adjacent subtropical gyres. In the Atlantic Ocean, SAMW and AAIW initially move northward with the Malvinas Current adjacent to the South American continent, but penetration into the subtropical gyre along the western boundary is blocked by the southward-flowing Brazil Current. SAMW and AAIW are eventually transported into the subtropical gyre at the eastern boundary when part of the South Atlantic Current (SAC) turns northward, feeding the Benguela Current (Stramma and Peterson 1990; Peterson and Stramma 1991).

SAMW and AAIW enter the Indian subtropical gyre at several sites across the basin at 32°S. The northward transport of SAMW and AAIW into the subtropical gyre is associated with weakening of the South Indian Ocean Current (SIOC) at 50°E, 65°E, 90°E, and 100°E into the Perth Basin (Stramma 1992; Fine 1993; Toole and Warren 1993). In the Pacific Ocean, the Subtropical Front (STF) and associated weak South Pacific Current (SPC) at 44°S form the boundary between the subtropical Pacific and the subantarctic zones (Stramma et al. 1995). The SPC moves gradually north across the Pacific basin. Reid (1986) shows an anticyclonic flow in the Pacific Ocean with a southward weak western boundary current and a broad northward flow across 40°S to the east of 170°W.

The northward transport of SAMW and AAIW from the South Atlantic, southern Indian Ocean, and South Pacific currents injects cold, fresh (hereafter C&F) mode and intermediate water into the respective subtropical ocean basins. In all the subtropical basins, SAMW and AAIW circulate in the wind-driven gyres. In the western Brazil, Agulhas, and East Australian Currents, modified warm, salty (hereafter W&S) mode and intermediate water are returned to the Southern Ocean. The exchange of ''new'' mode and intermediate water with ''older'' mode and intermediate water represents the mechanism by which antarctic upper waters ventilate the subtropical gyres.

The SAMW and AAIW are active participants in the global overturning and interbasin circulations (e.g., Schmitz 1995, 1996). The export of North Atlantic Deep Water (NADW) is largely balanced by northward transport of thermocline, mode, and intermediate water across 30°S in the Atlantic (Rintoul 1991). Somewhere, deep water must be converted to lighter water to close the loop, so the intermediate density waters of the Southern Hemisphere must be involved. SAMW and AAIW are also likely to play a part in the interbasin circulation associated with the Indonesian Throughflow. The throughflow must be fed by northward flow that enters the Pacific from the Southern Ocean. Schmitz (1996) suggests that the inflow is supplied by SAMW and AAIW. To accomplish these interbasin circulations, water masses must be converted from one density to another by air–sea buoyancy forcing or interior mixing.

However, although we have some knowledge of the circulation of SAMW and AAIW, their transports and the relative contributions of mixing and air–sea fluxes to the modification and renewal are still largely unknown. To address these issues—the primary goal of this study—it is essential to have a model that can include lateral, diapycnal, and air–sea fluxes in a physically consistent manner. Here we use an inverse model and hydrographic data to determine the three-dimensional circulation of SAMW and AAIW in the southern oceans south of about 12°S. Two novel features of the model make this possible. First, by including independent unknowns for the diapycnal flux of each property, the model can successfully determine net diapycnal fluxes in the ocean interior (McIntosh and Rintoul 1997; Sloyan and Rintoul 2000a). Second, we explicitly include air–sea fluxes of heat, freshwater, and momentum and the water mass transformations they drive (Tziperman 1986; Speer and Tziperman 1992; Sloyan and Rintoul 2000b).

This paper describes the circulation of thermocline and intermediate waters in each sector of the Southern Ocean. In section 2 a brief description of the design of the inverse model is given, including the treatment of diapycnal fluxes, model constraints, air–sea forcing, and error estimates. Section 3 compares the water mass transformation estimated from several air–sea flux climatologies and describes the corrections to the fluxes provided by the inverse solution. A detailed discussion

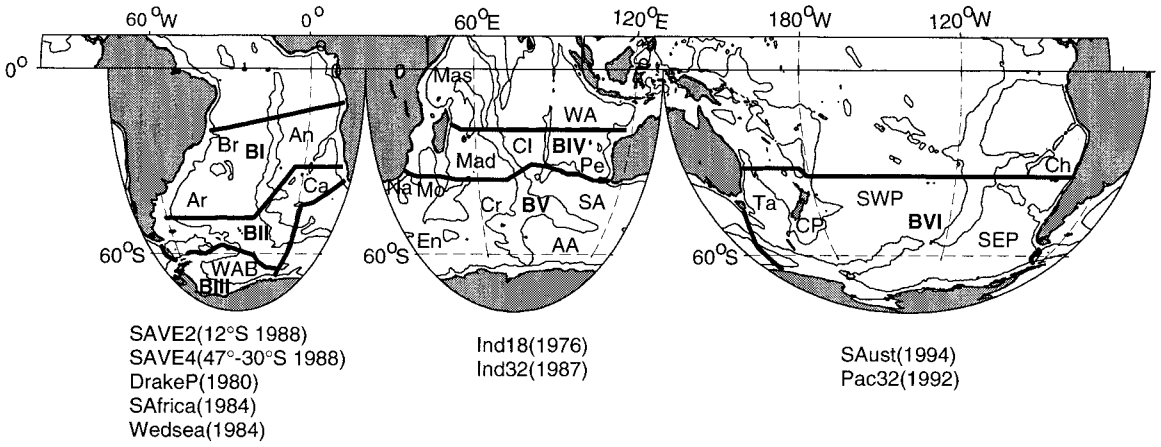

FIG. 1. Position and year of hydrographic sections and box regions used in the inverse model. The 3500-m isobath and the major bathymetric features are shown. Atlantic sector: Br, Brazil Basin; An, Angola Basin; Ar, Argentine Basin; Ca, Cape Basin; and WAB, Weddell abyssal plain. Indian Sector: Na, Natal Basin; Mo, Mozambique Basin; Mas, Mascarene Basin; Mad, Madagascar Basin; CI, Central Indian Basin; WA, West Australian Basin; Pe, Perth Basin; En, Enderby Basin; Cr, Crozet Basin; SA, South Australian Basin; and AA, Australian–Antarctic Basin. Pacific sector: Ta, Tasman Basin; CP, Campbell Plateau; SWP, Southwest Pacific basin; Ch, Chile Basin; and SEP, Southeast Pacific basin.

of the upper circulation in each basin and the renewal and modification of SAMW and AAIW is provided in section 4. Section 5 describes the role of mode and intermediate water in the global thermohaline circulation. The conclusions are summarized in section 6.

2. The inverse model

For completeness, a brief description of the inverse model is given below. [Most of this information is also given in Sloyan and Rintoul (2000a,b).]

a. Hydrographic data, domain, and layers

Nine hydrographic sections are used to define six ''boxes'' in the Southern Hemisphere oceans, as shown in Fig. 1. The sections used are recent (1984–94) high quality hydrographic sections, apart from the Ind18 section, which was occupied in 1976 (Sloyan and Rintoul 2000a,b). The sections across the Pacific, in Drake Passage, and south of Australia are part of the World Ocean Circulation Experiment (WOCE) dataset. Twenty-three layers are chosen to span the water masses in the model domain (Sloyan and Rintoul 2000b). The layers are defined by neutral density surfaces calculated using the Jackett and McDougall (1997) algorithm.

The temperature and salinity data are used to determine the baroclinic or relative velocity between adjacent stations along the hydrographic sections. Bottom triangle property transport is estimated by maintaining the horizontal density gradient at the deepest common depth of each station pair through the bottom triangle area. The Ekman property fluxes are calculated normal to the station pairs along the hydrographic section. The depth of the Ekman layer is assumed to be 60 dbar for all sections, and the Ekman flux is calculated using Hellerman and Rosenstein (1983) annual mean wind stress.

Across the meridional sections (SAVE2, SAVE4, Ind18, Ind32, and Pac32), the initial reference level is the boundary between the northward flowing Antarctic Bottom Water (AABW) and southward flowing NADW, Indian Deep Water (IDW), and Pacific Deep Water (PDW). In the Argentine Basin of SAVE 4 and the three Southern Ocean choke point sections (DrakeP, SAfrica, and SAust), the initial reference level is taken to be the deepest common depth at each station pair.

b. Model constraints, weighting, and error estimates

A box inverse model, following that of Wunsch (1978) is designed. Mass, heat, and salt are conserved in all layers while the silica constraint is imposed as a total box constraint. Two aspects of the inverse model are new: we use independent diapycnal flux unknowns for each property [mass (w_m), heat (w_h), and salt (w_s)] and explicitly include air–sea fluxes of heat, freshwater, and momentum (wind) and the water mass transformation they drive.

The inclusion of independent diapycnal fluxes for each property represents the net diapycnal flux that results from all mixing processes that act to transfer mass, heat, or salt between water masses in the ocean interior. (Here, ''interior'' is taken to mean the entire ocean beneath the sea surface. Diapycnal fluxes across isopycnals outcropping in the surface mixed layer, for example, are included in the interior diapycnal fluxes). These mixing processes include advection, diffusion, cabbeling, and eddy fluxes.

Exchange of heat and freshwater with the atmosphere results in net buoyancy forces that can transfer fluid

from one density layer to another (Walin 1982). To date, inverse methods have not explicitly included these effects on the mass, heat, or salt conservation equations. Inverse models usually either downweight the conservation requirement in layers that outcrop and interact with the overlying atmosphere or only consider conservation below the thermocline (Metzl et al. 1990; Rintoul 1991; Macdonald 1998). Rather than discard the information contained in the conservation constraints for outcropping layers, it is desirable to include the effects of air–sea interaction explicitly. This is particularly so at high latitudes, where many layers outcrop. More importantly, the diapycnal fluxes driven by air–sea interaction are a fundamental part of the three-dimensional circulation of the ocean. An inverse model that seeks to determine this circulation should include these processes in a physically consistent manner.

The effect of air–sea fluxes of heat, freshwater, and momentum can be included explicitly in the model following the strategy of Walin (1982), Tziperman (1988), Schmitt et al. (1989), and Speer and Tziperman (1992). The mass flux (f_m) due to air–sea fluxes of heat and freshwater and Ekman transport is

$$f_m = \frac{-\alpha H}{C_p} + \rho\beta QS - \rho Q + \frac{d(E\rho)}{d\rho}. \quad (1)$$

In Eq. (1), ρ is the sea surface density, α is thermal expansion coefficient, β is saline contraction coefficient, H is heat flux, Q is freshwater flux (evaporation minus precipitation minus runoff), S is sea surface salinity, E is Ekman transport, and C_p is specific heat. Each of these terms is a function of time and position. The first two terms of Eq. (1) represent the effect of heat and freshwater fluxes on density, while the last two terms are direct input/loss of freshwater and the horizontal Ekman transport, respectively. The total mass flux across an isopycnal with density ρ, for one year, as a function of sea surface density is

$$F_m(\rho) = \int_{\text{year}} dt \iint_{\text{area}} dA f_m \delta(\rho - \rho'), \quad (2)$$

where the δ function samples the density flux at surface ρ. The mass convergence in a layer bounded by isopycnals ρ and $\rho + d\rho$ is

$$C_m(\rho)d\rho = -[F_m(\rho + d\rho) - F_m(\rho)]. \quad (3)$$

In a similar manner, the convergence of heat and salt in density layers due to air–sea fluxes of heat, freshwater, and momentum can be found.

The heat flux (f_h) across outcropping density surfaces is

$$f_h = \frac{-H}{C_p\rho} + \frac{d(E\theta_{\text{De}}\rho)}{d\rho}, \quad (4)$$

while the salt flux (f_s) is

$$f_s = \frac{d(ES_{\text{De}}\rho)}{d\rho}, \quad (5)$$

where θ_{De} and S_{De} are the weighted mean temperature and salinity over the Ekman layer (De).

The mass, heat, and salt fluxes across each outcropping layer are calculated from climatological datasets. Because the data are discontinuous, the property transformations across outcropping neutral density surfaces are summed over a discrete interval surrounding the outcropping density (Speer and Tziperman 1992). The delta function is now a boxcar (Π) of width $\Delta\rho$:

$$F_m(\rho) = \sum_{n=1}^{12} \Delta t \sum_{i,j} \Delta A_{i,j} \times \left[\frac{1}{\Delta\rho}\left(\frac{-\alpha H^n_{i,j}}{C_p} + \rho\beta Q^n_{i,j} S\right) - Q^n_{i,j} + E^n_{i,j}\right] \times \Pi(\rho - \rho') \quad (6)$$

$$F_h(\rho) = \sum_{n=1}^{12} \Delta t \sum_{i,j} \Delta A_{i,j}\left[\frac{H^n_{i,j}}{C_p\rho} + E^n_{i,j}\theta_{\text{De}_{i,j}}\right]\Pi(\rho - \rho') \quad (7)$$

$$F_s(\rho) = \sum_{n=1}^{12} \Delta t \sum_{i,j} \Delta A_{i,j} \sum_{n=1}^{12} [E^n_{i,j} S_{\text{De}_{ij}}]\Pi(\rho - \rho'). \quad (8)$$

The climatological data used for the air–sea fluxes are heat flux (H) Comprehensive Ocean–Atmosphere Data Set (COADS) by da Silva et al. (1994), wind stress (E) Hellerman and Rosenstein (1983) and, freshwater (Q) from the Global Assimilation and Prediction System by Budd et al. (1995). We use Levitus and Boyer (1994) to find the outcropping position of the neutral density surfaces for each month, the weighted mean Ekman layer temperature and salinity, and the annual mean depth and property concentration of the neutral density surfaces found within each box.

The datasets used to calculate the air–sea fluxes contain errors, including errors in the bulk formulae used and a lack of oceanographic and meteorological observations, especially at high latitudes and over subtropical regions away from commercial shipping routes (Speer and Tziperman 1992; Barnier et al. 1995). As a result, we treat these climatologies as an initial guess in the inverse model and use the inverse solution to determine corrections to the climatological datasets, which make them consistent with the hydrographic data and the model physics. Unfortunately, no errors are given with the air–sea climatologies. We assign an arbitrary a priori error of 10%–20% to the air–sea flux climatologies. Our solution can be interpreted as a test of the consistency between present best estimates of these fluxes, the hydrography, and the model constraints. The inverse solution is examined carefully to ensure that the inverse-corrected air–sea fluxes, diapycnal fluxes, and lateral fluxes are compatible with our present understanding of the circulation.

The conservation equations, including the diapycnal

TABLE 1. A priori constraints (+ve: north/eastward), uncertainties applied to the inverse model and inverse estimate. The inverse model conserves mass, heat, and salt in all layers, while silica is conserved in each box as a whole.

Constraint		Model
$-0.8 \pm 2 \times 10^6$ m^3 s^{-1}	Net southward transport at SAVE2 (Coachman and Aagaard 1988)	$-0.77 \pm 2.9 \times 10^6$ m^3 s^{-1}
$4 \pm 2 \times 10^6$ m^3 s^{-1}	Northward bottom water transport in Brazil Basin (Hogg et al. 1982; Speer and Zenk 1993)	$5 \pm 2 \times 10^6$ m^3 s^{-1}
$0 \pm 2 \times 10^6$ m^3 s^{-1}	Net transport across Wedsea	$-0.4 \pm 2.5 \times 10^6$ m^3 s^{-1}
16 ± 5 W m^{-2}	Heat loss over Weddell Sea (Gordon and Huber 1990; Fahrbach et al. 1994)	15.5 ± 3 W m^{-2}
$60 \pm 5 \times 10^6$ m^3 s^{-1}	Northward Malvinas Current (Peterson and Stramma 1991; Peterson 1992)	$57.7 \pm 3.2 \times 10^6$ m^3 s^{-1}
$6 \pm 2\ 10^6$ m^3 s^{-1}	Northward transport AABW across Argentine Basin (Whitworth et al. 1991)	$6 \pm 2 \times 10^6$ m^3 s^{-1}
$11 \pm 5 \times 10^6$ m^3 s^{-1}	Northward transport AABW/LCDW coincident with WOCE PCM-9 (Pac32 between 181° and 192.5°E) (Whitworth et al. 1999)	$11.2 \pm 1 \times 10^6$ m^3 s^{-1}
Silica O(1000 kmol s^{-1})	Conservation all regions (Trèguer et al. 1995)	Conservation O(500–1000 kmol s^{-1})

flux unknowns for each property and the air–sea flux-driven transformations, take the form

$$\sum_{j=1}^{N} \Delta x_j \int_{h_m}^{h_{m+1}} \rho C_j (\upsilon_r + b)_j \, dp + E_j \rho C_j + (w_c A \rho C)_m - (w_c A \rho C)_{m+1} + (F_c + F_c^*)_m - (F_c + F_c^*)_{m+1} = 0. \quad (9)$$

In Eq. (9) Δx_j is the station spacing at pair j, and C_j is the property value/unit mass at pair j. The baroclinic or relative velocity (υ_{r_j}) is determined from the hydrographic data, $E_j C_j$ is the Ekman property flux at pair j, and F_c is the total flux across an outcropping isopycnal driven by buoyancy forcing. The subsequent system of simultaneous equations is solved for the unknown reference level velocities (b), the diapycnal fluxes for mass, heat, and salt (w_m, w_h, w_s), and the corrections to the air–sea flux (F_c^*) [Eq. (9)]. The total system comprises 281 equations and 1794 unknowns.

Table 1 contains information on the a priori constraints applied to the inverse model. No prior constraint is placed on the transport of the ACC. Total silica conservation in each box is a weak constraint, reflecting the uncertainty in the silica flux. Salt conservation equations are written as anomaly equations, salinity − 35 psu. The rows are weighted by the property norm and the columns are weighted by the area norm. A scaling factor is also applied to the reference velocity unknowns, the diapycnal property flux unknowns, and air–sea climatology corrections such that the condition number (the ratio of largest eigenvalue to smallest eigenvalue) is minimized (McIntosh and Rintoul 1997). Errors due to the combination of nonsynoptic hydrographic sections leads us to choose a rank (262) where the residuals are mass O[(1 to 2) $\times 10^6$ m^3 s^{-1}], heat O[(2–5) $\times 10^6$ m^3 s^{-1} $\times$ mean layer temperature], salt O[(2–5) $\times 10^6$ m^3 s^{-1} $\times$ mean layer salt], and silica O(1000 kmol s^{-1}).

The error bars presented are the sum of the noise and null space errors, which are calculated following Wunsch et al. (1983) and Rintoul (1991). These errors represent the formal errors of the inverse method—the error associated with determining the barotropic velocity and diapycnal fluxes. These formal errors do not take into account errors due to the asynoptic data, solution sensitivity to the first guess, and ocean variability. As the formal errors do not include these other error sources, they are unlikely to reflect the true uncertainty in the estimates. In recognition of the inadequacy of the formal error bars, Macdonald and Wunsch (1996) and Macdonald (1998), for example, chose to increase the uncertainty of all their heat flux estimates by a somewhat arbitrary ±0.25 PW [based on Holfort (1994) error analysis in the South Atlantic]. They believed that this value more accurately accounted for the effect of (the unmeasured) oceanic variability. The value used is much larger than the formal error bar provided by the inverse method. Here we have chosen to present the estimates with the formal error bars so that it is clear what the error bars represent. If a good estimate exists of the uncertainty introduced by error sources not included in the formal error bars (e.g., Holfort's value of 0.25 PW for the South Atlantic), this value should be added to the error bars shown here.

Ultimately, better assessments of the uncertainty in ocean flux estimates, however made, require measurements of ocean variability (and forcing), which do not yet exist for most of the ocean. One exception is the WOCE SR3 section south of Australia, which was occupied six times between 1991 and 1996, including each season. Sloyan (1997) tested the sensitivity of the inverse solution by rerunning the model using a realization of the SR3 section from a different year and different season (winter 1995). Overall, the changes were small (layer transport changes of $<1 \times 10^6$ m^3 s^{-1} in almost all layers, and usually $<0.5 \times 10^6$ m^3 s^{-1}, except at the SR3 section itself). The main difference from the

solution described below is an increase of 5×10^6 m^3 s^{-1} in the eastward flow south of Australia, which is balanced by increased northward flow in the Pacific, increased Indonesian Throughflow, and increased southward flow in the Indian Ocean. The increased transport across the Indian and Pacific sections is mostly achieved by small, $\leq 1 \times 10^6$ m^3 s^{-1}, changes that are evenly distributed throughout the water column. The differences at SR3 represent both seasonal and longer timescale variability. The seasonal variability is largest, $\sim 6 \times 10^6$ m^3 s^{-1}, in the shallowest layers (10–14), which are present in the summer realization but are absent or occupy a smaller area in the winter realization. In the deep and bottom layers, the difference between the two SR3 realizations are an indication of interannual variability and are generally $\leq 2 \times 10^6$ m^3 s^{-1}. The overall increase in the transport across the Indian and Pacific sections, in response to a different realization of SR3, would suggest a variability for this circulation path of $\pm 5 \times 10^6$ m^3 s^{-1}. Note, however, that the net heat flux across roughly 30°–40°S (SAVE4, Ind32, and Pac32) is almost unchanged (SAVE4 0.32 ± 0.05, Indian 32°S 1.06 ± 0.07, Pacific 32°S 0.26 ± 0.05, and a net difference of 0.02 PW), despite the increase in strength of the circum-Australia flow. While using different realizations of a single section clearly does not provide a complete assessment of the impact of oceanic variability on our circulation estimates, the sensitivity test supports the assumption that robust estimates of the large-scale circulation and fluxes can be made from models such as the one used here.

3. Transformation by air–sea fluxes

Figures 2, 3, and 4 show the initial and inverse corrections to the air–sea Ekman, heat, and freshwater components of the transformation at outcropping neutral density surfaces. Also shown are the estimated transformations from climatologies not used in this inverse model. In general the inverse corrections to the air–sea Ekman, heat, and freshwater fluxes are small. The European Centre for Medium-Range Weather Forecasts (ECMWF; Trenberth et al. 1990) and Hellerman and Rosenstein (1983) Ekman transformations show a similar pattern (Fig. 2), but the ECMWF winds show a larger northward Ekman flux (towards lighter neutral density layers) over the Southern Ocean sectors (Boxes II, V, VI).

A comparison of the heat flux contribution to transformation between the COADS and ECMWF heat climatologies shows a variation in both size and direction of the air–sea flux. ECMWF heat climatology has a larger heat gain over the lighter outcropping layers in the Southern Ocean in comparison to COADS heat flux. This results in larger northward flux (toward light density layers) across layers 7–10 in the Atlantic sector, 7–14 in the Indian sector, and 7–10 in the Pacific sector. At higher latitudes (layers 13–16), the ECMWF heat climatology estimates a larger heat loss and a larger southward transformation (to denser layers) in the Indian and Pacific sectors compared to the COADS heat climatology.

ECMWF (Keith 1995), Baumgartner and Reichel (1975), and GASP-corrected freshwater transformations show a similar pattern in both magnitude and direction (Fig. 4). The largest difference between the climatologies occurs in the subtropical Atlantic (Box I) and Southern Ocean Atlantic sector (Box II). In the subtropical Atlantic, the ECMWF freshwater climatology has a stronger evaporation loss and subsequent larger transformation of lighter water to denser water compared to GASP corrected and Baumgartner and Reichel. In the Southern Ocean Atlantic sector, Baumgartner and Reichel show a much stronger evaporation of freshwater, which results in a significantly larger transformation of lighter layers to denser water masses (layers 7–9), over that of the GASP-corrected and ECMWF freshwater fluxes.

Although there is some variation in the estimated air–sea transformation between climatologies, all suggest that air–sea forcing results in a significant flux of water from one density to another. As stated, the errors given in the paper are the formal errors of the inverse method. Figures 2, 3, and 4 provide some indication of the uncertainty in the air–sea transformation due to differences between the wind, heat, and freshwater climatologies. A comparison of the estimated air–sea fluxes for each component of the mass transformation suggests a net mass transformation variability of $10–20 \times 10^6$ m^3 s^{-1} between the climatologies.

4. Circulation of AAIW and SAMW in individual basins

In this section the circulation of surface (layers 1–6), thermocline (layers 7–9), and intermediate water (layers 10–14) is described for each sector of the southern oceans. Table 2 gives the net horizontal mass transports across each hydrographic section, and Fig. 5 is a schematic diagram of the overturning circulations in each basin and their zonal integral. In general, Bottom Water (BW) and Lower Deep Water (LDW, which incorporates NADW) are exported to the subtropical Indian and Pacific Oceans. These waters are returned to the Southern Ocean as Upper Deep Water (UDW). The deep cell is closed at high latitudes by conversion of UDW to BW/LDW [see Sloyan and Rintoul (2000b)]. UDW also participates in an upper deep–intermediate water (IW) cell. UDW upwells at high latitude and is driven north in the Ekman layer, where it is transformed to lighter water by air–sea buoyancy fluxes. One of the main aims of this paper is to quantify the flow paths and relative roles of transformation and diapycnal mixing involved in the UDW–IW cell.

The explicit inclusion, in this model, of air–sea fluxes and the transformation they drive shows that UDW up-

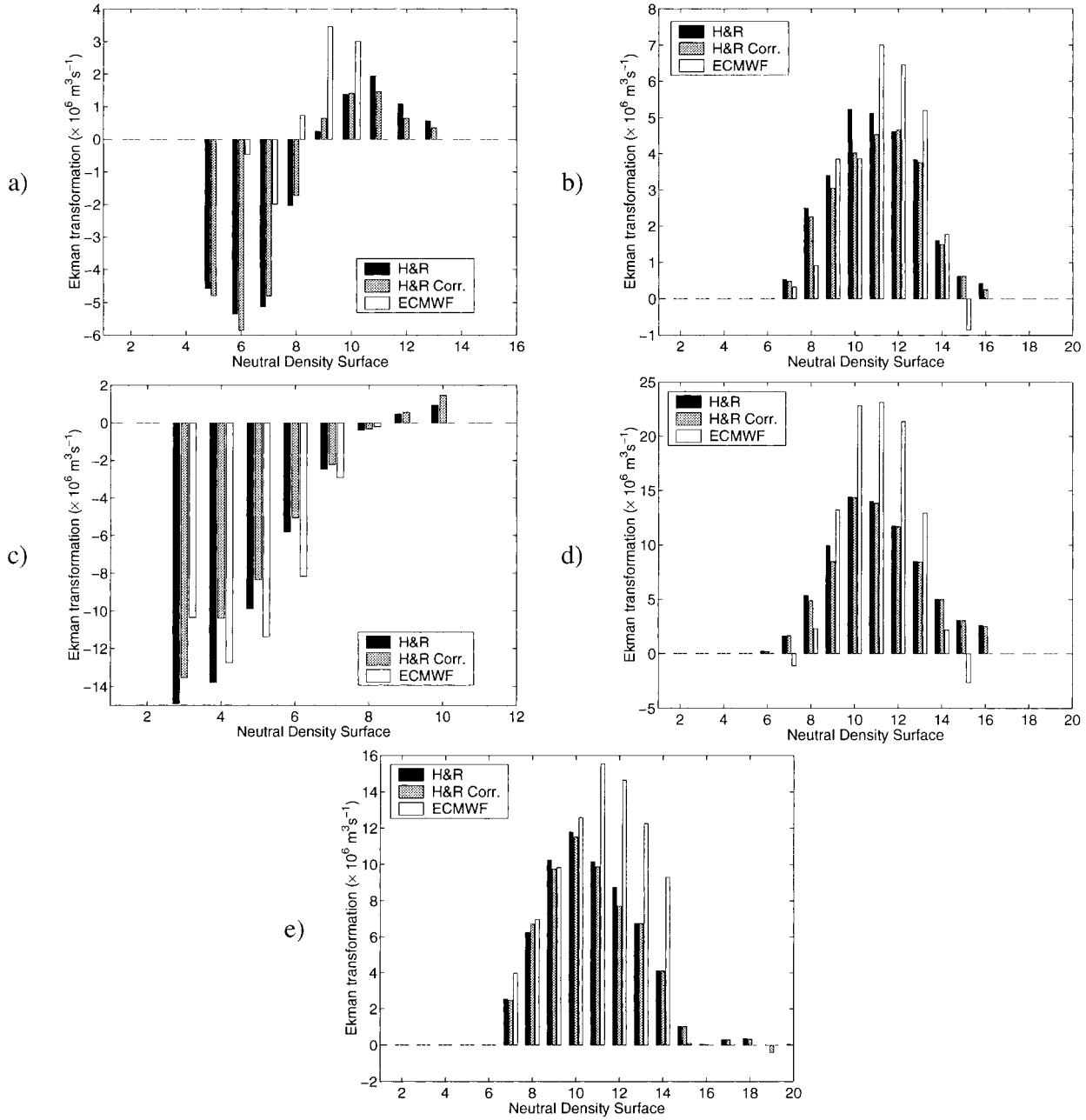

FIG. 2. Ekman component to the mass transformation, Hellerman and Rosenstein (H&R; 1983), inverse correction H&R, and comparison with ECMWF (Trenberth et al. 1990) Ekman fluxes for outcropping layers in the (a) subtropical Atlantic (Box I), (b) Southern Ocean Atlantic sector (Box II), (c) subtropical Indian (Box IV), (d) Southern Ocean Indian sector (Box V), and (e) Southern Ocean Pacific sector (Box VI).

wells at high latitude and is driven north in the Ekman layer. The influence of the air–sea transformation of UDW to intermediate water is the subject of this paper.

a. Atlantic sector

1) HORIZONTAL CIRCULATION

The circulation of the upper layers of the subtropical Atlantic is dominated by the currents that together form the subtropical gyre: poleward flow in the Brazil Current along the western boundary, eastward flow in the South Atlantic Current, equatorward flow in the Benguela Current in the eastern basin, and westward flow at lower latitudes in the gyre interior.

Figure 6 summarizes the transport of surface/thermocline water, SAMW, and AAIW across each of the Atlantic sections. [The lightest water (layer 5) in the Atlantic is denser than the lightest four layers of the

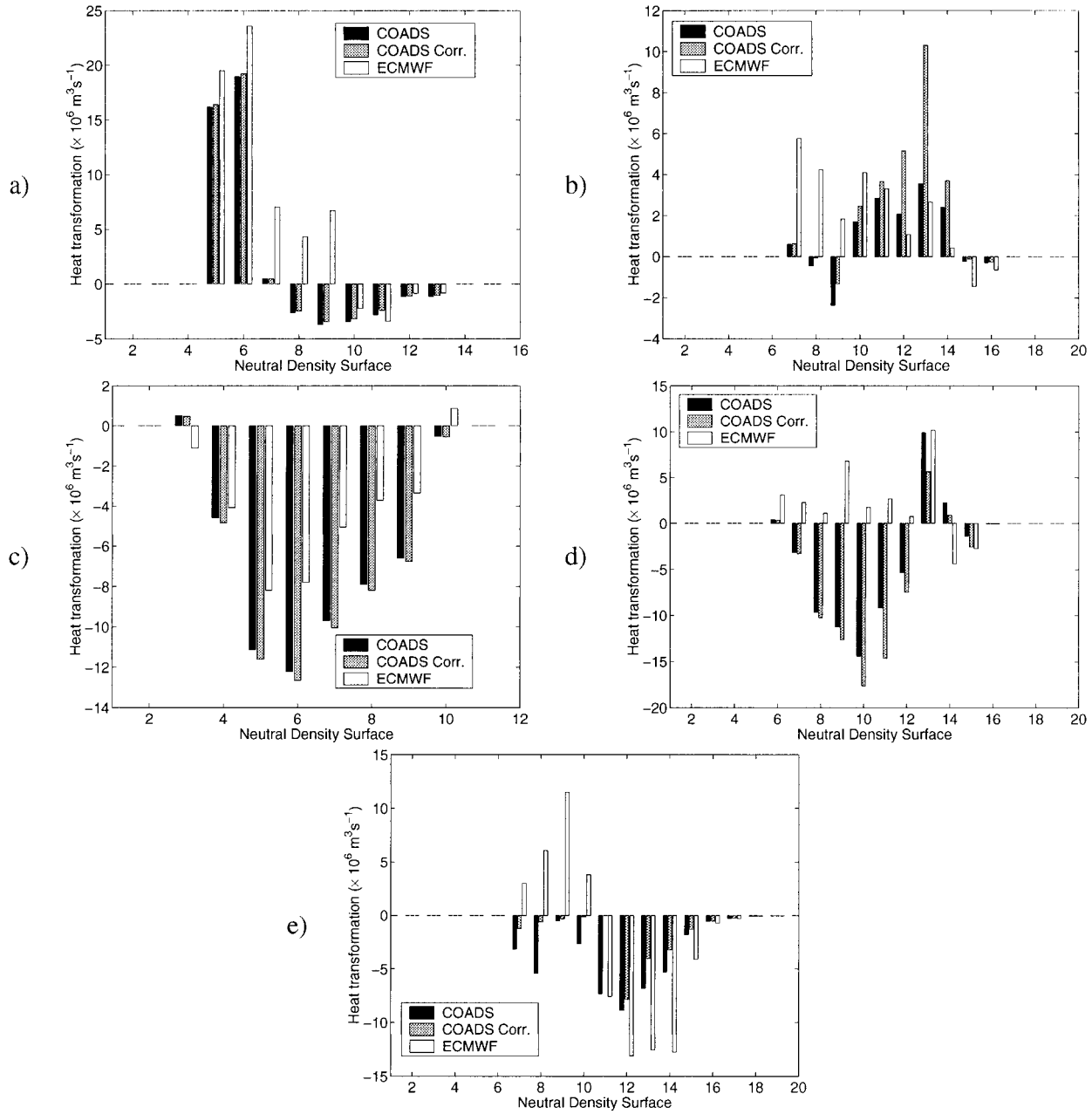

FIG. 3. Heat component to the mass transformation, COADS, inverse correction to COADS, and comparison with ECMWF (Barnier et al. 1995) heat transformation for outcropping layers in the (a) subtropical Atlantic (Box I), (b) Southern Ocean Atlantic sector (Box II), (c) subtropical Indian (Box IV), (d) Southern Ocean Indian sector (Box V), and (e) Southern Ocean Pacific sector (Box VI).

model ($\gamma^n \leq 23.5$).] At SAVE2, the beginning of the shallow weak ($2.6 \pm 0.4 \times 10^6$ m^3 s^{-1}) southward Brazil Current is seen adjacent to the western boundary (Fig. 6). (Recall that the quoted errors are the formal error of the inverse method and therefore are unlikely to reflect the true uncertainty in estimates.) The southward flow of the Brazil Current is more than compensated by northward transport of $5.9 \pm 0.5 \times 10^6$ m^3 s^{-1} of thermocline water, principally in the Brazil Basin.

Figure 7 shows the temperature and neutral density distribution along SAVE4. Across SAVE4 a small amount, $1.8 \pm 0.2 \times 10^6$ m^3 s^{-1}, of thermocline water moves southeastward across the Mid-Atlantic Ridge (Fig. 6). This flux of thermocline water, together with $1.8 \pm 0.1 \times 10^6$ m^3 s^{-1} of thermocline water flowing westward south of Africa, results in a $3.4 \pm 0.7 \times 10^6$ m^3 s^{-1} northward flow in the Benguela Current (Fig. 6). Saunders and King (1995) estimate a northward transport of surface water of 10×10^6 m^3 s^{-1} at 30°–45°S, and Macdonald (1998) estimates a northward transport

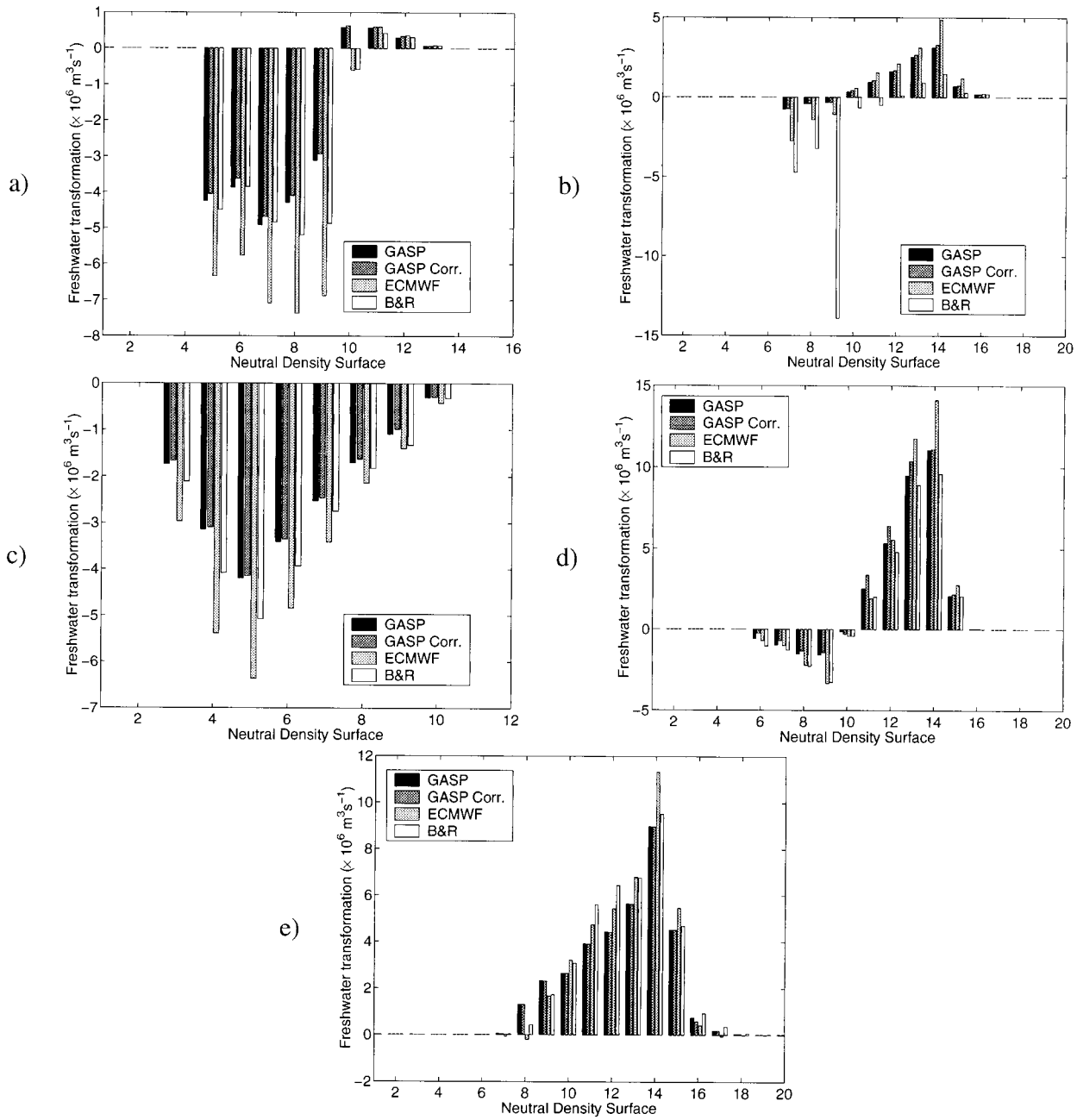

FIG. 4. Freshwater component to the mass transformation, GASP, inverse correction to GASP, and comparison with ECMWF (Keith 1995) and Baumgartner and Reichel (B&R; 1975) freshwater transformations for outcropping layers in the (a) subtropical Atlantic (Box I), (b) Southern Ocean Atlantic sector (Box II), (c) subtropical Indian (Box IV), (d) Southern Ocean Indian sector (Box V), and (e) Southern Ocean Pacific sector (Box VI).

of 13 ± 1 × 10^6 m^3 s^{-1} at 11°S and 7 ± 1 × 10^6 m^3 s^{-1} at 23°S. Differences in the fluxes of surface/thermocline water result in part from the inclusion of our lightest SAMW in surface/thermocline water by Saunders and King (1995) and Macdonald (1998).

At Drake Passage, 32.7 ± 0.5 × 10^6 m^3 s^{-1} of intermediate water (4.8 × 10^6 m^3 s^{-1} of SAMW and 27.9 × 10^6 m^3 s^{-1} of AAIW) enters the Atlantic sector (Fig. 6). The large transport of AAIW relative to SAMW reflects the fact that lighter SAMW occupies only a small portion of the section. In the Argentine Basin at 47°S, 27.8 ± 1 × 10^6 m^3 s^{-1} of SAMW/AAIW flow northward (Fig. 6). Adjacent to the South American coast, the Malvinas Current continues northward to between 38°S and 33°S, then turns offshore to form the SAC (Stramma and Peterson 1990). The SAC moves

TABLE 2. Total section property fluxes (+ve: northward/eastward). Heat fluxes are relative to 0°C and converted to PW (1 PW = 244 × 10^{6}°C m^3 s^{-1}). Units are mass × 10^6 m^3 s^{-1}, heat PW × 10^{15}W, salt × 10^6 kg s^{-1}, freshwater × 10^9 kg s^{-1}, and silica kmol s^{-1}.

Section	Mass	Heat	Salt	Freshwater	Silica
SAVE2	−0.77 ± 2.9	0.42 ± 0.05	−28.3 ± 29.5	−0.85 ± 3.0	124 ± 194
SAVE4	−0.80 ± 2.7	0.28 ± 0.04	−27.6 ± 55.5	−0.83 ± 2.9	295 ± 339
DrakeP	134.9 ± 0.75	1.41 ± 0.01	4785.9 ± 14.1	134.2 ± 0.83	9071 ± 73
SAfrica	135.4 ± 2.7	1.19 ± 0.03	4795.1 ± 51.7	134.5 ± 2.8	8450 ± 407
Weddell Sea	−0.35 ± 2.5	−0.05 ± 0.01	−13.7 ± 57.3	−0.35 ± 2.6	−26 ± 339
Ind18	−10.4 ± 3.1	−1.27 ± 0.05	−371.7 ± 56.3	−10.3 ± 3.0	261 ± 679
Ind32	−10.3 ± 2.3	−0.87 ± 0.06	−369.1 ± 43.9	−10.2 ± 2.4	425 ± 316
SAust	145.6 ± 1.0	1.83 ± 0.01	5164.4 ± 18.8	144.7 ± 1.2	8017 ± 99
Pac32	7.4 ± 1.8	0.13 ± 0.04	261.1 ± 43.7	7.32 ± 2.0	821 ± 283

eastward across the mid-Atlantic ridge, transporting 42.1 ± 2 × 10^6 m^3 s^{-1} of modified and recirculating SAMW and AAIW southeastward across SAVE4 into the Southern Ocean Atlantic sector (Fig. 6).

There is an increase in transport of 3.2 × 10^6 m^3 s^{-1} in SAMW between the eastward transport at Drake Passage and the northward transport in the Argentine Basin, and a further convergence of 9.6 × 10^6 m^3 s^{-1} between the Malvinas Current and the Mid-Atlantic Ridge. The increase in transport of SAMW in the southwest Atlantic (Box II) is the result of air–sea fluxes, which convert 8.4 ± 1 × 10^6 m^3 s^{-1} of C&F AASW ($\theta < 2$°C and $S < 34$) to SAMW (Fig. 6, discussed below). In the western part of the subtropical basin (Box I), the increased transport of SAMW results from a combination of a small interior diapycnal flux of denser AAIW into SAMW, an air–sea transformation of thermocline water to SAMW (discussed below), and the inclusion of recirculating ''old'' SAMW within the subtropical gyre.

AAIW that enters the Atlantic sector from the Pacific sector bifurcates just east of Drake Passage, with 19.8 × 10^6 m^3 s^{-1} moving northward with the Malvinas Current and the remaining 8.1 × 10^6 m^3 s^{-1} continuing eastward with the ACC. In the subtropical region, the southeastward flow of AAIW across the Mid-Atlantic Ridge is increased over that which moves northward in the Malvinas Current by a small net interior diapycnal flux of NADW into AAIW and the recirculating salty AAIW in the subtropical gyre (Fig. 6).

The thermocline water, SAMW, and AAIW that balance the southward flow of NADW begin their journey north in the Benguela Current, which transports 16.4 ± 1 × 10^6 m^3 s^{-1} of SAMW and 5.8 ± 0.5 × 10^6 m^3 s^{-1} of AAIW northward in the Cape Basin (Fig. 6). SAMW and AAIW are carried to the northwest by the subtropical gyre between SAVE4 and SAVE2. At 12°S (SAVE2), 10.2 ± 0.5 × 10^6 m^3 s^{-1} of SAMW and 5.7 ± 0.7 × 10^6 m^3 s^{-1} of AAIW move northward in the Brazil Basin (Fig. 6). A smaller southward flow of 3.9 ± 0.6 × 10^6 m^3 s^{-1} of SAMW and 1.2 ± 1 × 10^6 m^3 s^{-1} of AAIW occurs in the Angola Basin (Fig. 6). Suga and Talley (1995) find a low-salinity, high-oxygen tongue extending eastward south of the equator that may feed the southward flow of SAMW and AAIW found in this model.

The upper circulation of the subtropical Atlantic and Southern Ocean Atlantic sector described above is in general agreement with previous regional or complete ocean basin studies (Reid 1989; Piola and Gordon 1989; Peterson and Stramma 1991; Saunders and King 1995; Schmitz 1995, 1996). Macdonald (1998), 11°S, has larger northward transports of surface/thermocline water and intermediate water, which essentially balance the southward transport of 23 × 10^6 m^3 s^{-1} of NADW. In this study, at 12°S, the northward transport of surface/thermocline water and intermediate water balance a smaller (18 × 10^6 m^3 s^{-1}) southward transport of NADW.

2) DIAPYCNAL FLUXES

Air–sea fluxes transform 6 ± 1 × 10^6 m^3 s^{-1} of W&S thermocline water (layer 9) to SAMW (layers 10–12) (Fig. 6). This transformation is more than compensated by a conversion of 8 ± 3 × 10^6 m^3 s^{-1} of SAMW into thermocline water by interior mixing. The diapycnal flux due to mixing occurs as SAMW circulates in the subtropical gyre. (In this study, ''ocean interior'' means everything below the sea surface and includes, e.g., horizontal mixing across outcropping density surfaces in the mixed layer.) Across the lower boundary of AAIW (neutral surface 14, $\gamma^n = 27.4$), in the subtropical gyre, there is an interior diapycnal flux of 4 ± 3 × 10^6 m^3 s^{-1} from Upper Circumpolar Deep Water (UCDW)/NADW, some of which (2 ± 2 × 10^6 m^3 s^{-1}) is further transferred to SAMW. The sum of the diapycnal fluxes due to transformation and interior mixing result in a small transfer of SAMW and AAIW to lower-thermocline water in the subtropical gyre.

While the diapycnal mass fluxes due to air–sea forcing and interior mixing in the subtropical Atlantic (Box I) tend to compensate each other in the thermocline and intermediate water, the diapycnal fluxes of heat and salt by these processes transfer heat and salt from the thermocline into the cold, fresh intermediate water. These diapycnal fluxes of heat and salt, along with isopycnal mixing between the new and recirculating intermediate water from the subtropical gyre, modify the *T–S* properties of intermediate water between Drake Passage and the Mid-Atlantic Ridge (Sloyan and Rintoul 2000a).

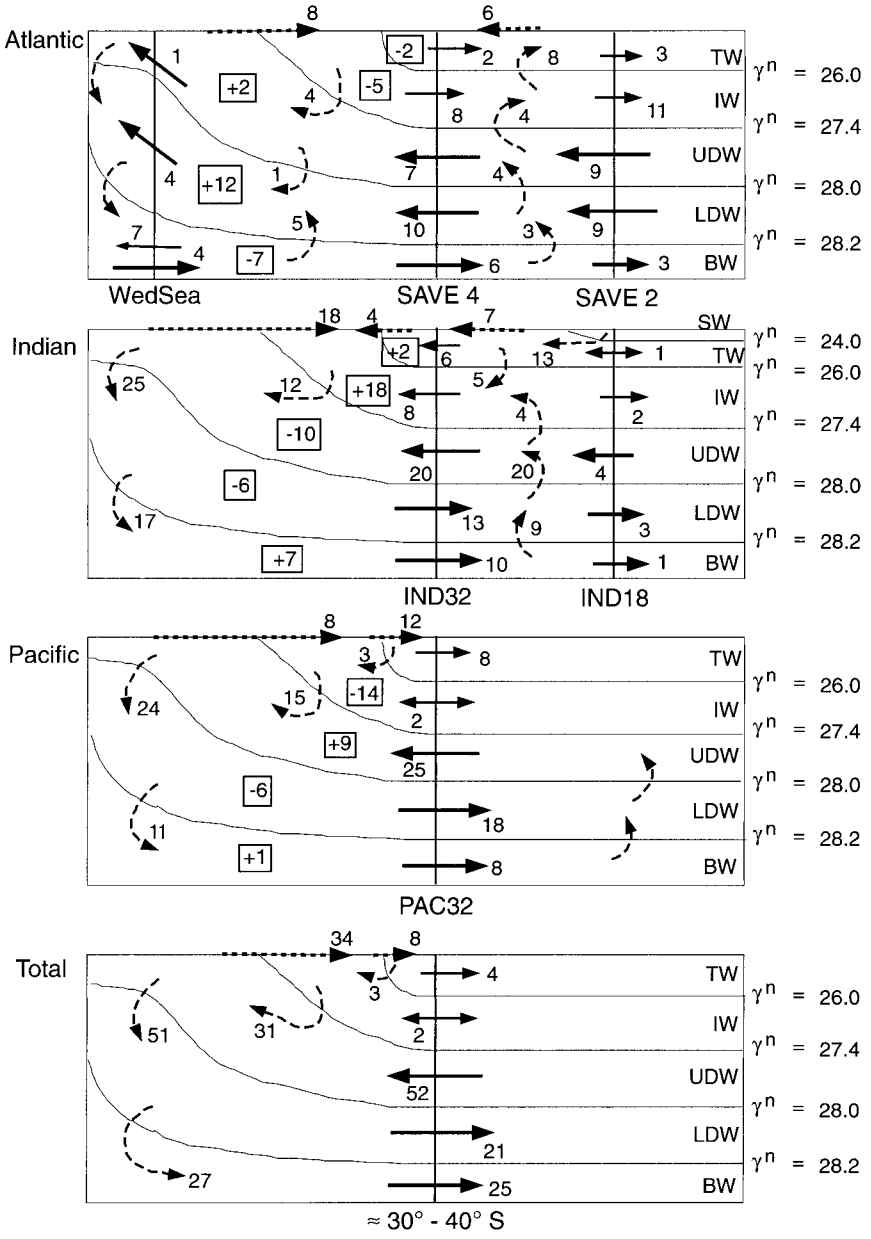

FIG. 5. A schematic five-layer view of the overturning circulation ($\times 10^6$ m^3 s^{-1}) in each Southern Hemisphere basin, and the zonal sum. SW: surface water, TW: thermocline water, IW: intermediate water, UDW: upper deep water, LDW: lower deep water, and BW: bottom water. The neutral density surfaces used to define each layer are shown. Air–sea flux driven diapycnal fluxes are shown by bold, dashed arrows at the sea surface. Diapycnal fluxes due to interior mixing are indicated by thin dashed arrows. Fluxes in boxes represent the net convergence (+ve) or divergence (−ve) of a particular water mass in that sector of the Southern Ocean due to meridional and diapycnal fluxes; mass is conserved by a compensating divergence in zonal transport of the ACC. Two-headed arrows in intermediate water highlight that the net flux is the difference of nearly balancing northward and southward fluxes. Small (2–3 $\times$ 10^6 m^3 s^{-1}) imbalances result from choosing a solution where layer residual norms are of O(1–2 $\times$ 10^6 m^3 s^{-1}) and rounding to nearest whole number (from Sloyan and Rintoul 2000b).

Numerous layers outcrop in the Atlantic sector of the Southern Ocean (Box II). The outcropping of UCDW (layers 15–17) south of the Polar Front exposes it to air–sea heat and freshwater fluxes that modify the temperature and salinity properties, resulting in the formation of C&F AASW. Across the APF zone, which includes both the Polar and Subantarctic Fronts, 8.4 $\pm$ 1 $\times$ 10^6 m^3 s^{-1} of AASW is modified by air–sea pro-

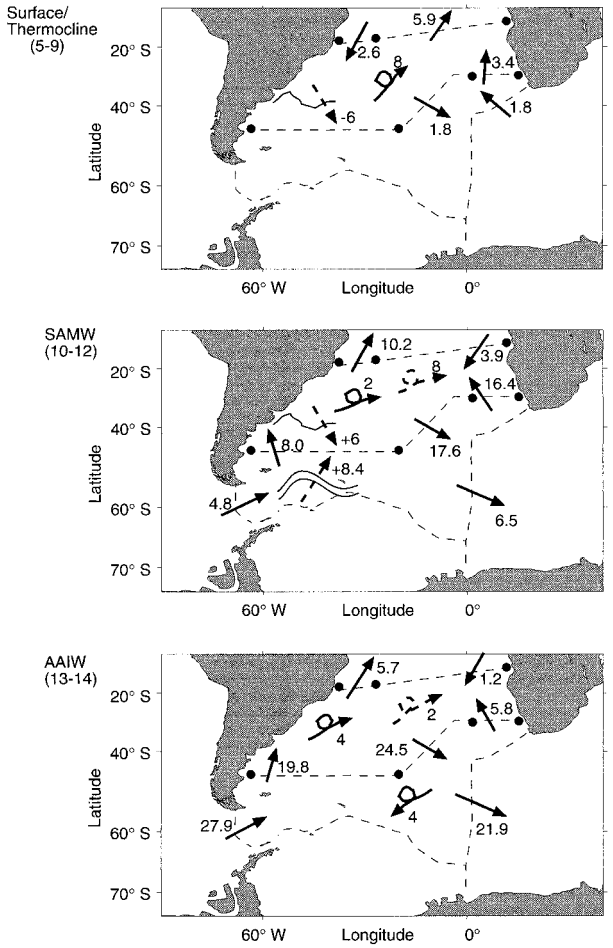

FIG. 6. Lateral and diapycnal volume fluxes ($\times 10^6$ m^3 s^{-1}) in thermocline and intermediate layers for the Atlantic region (Box I and II). Lateral fluxes (solid arrows) are shown for part of a section between ●, otherwise total flow across section. Interior diapycnal fluxes are curly arrows, with solid arrow indicating flux across lower interface and dashed arrow flux across upper interface. An upward (downward) diapycnal flux arrow represents upwelling (downwelling) across the interface. Air–sea diapycnal fluxes are dashed arrows angled across the outcropping interface between the water masses, with a positive (negative) value representing an air–sea buoyancy flux gain (loss). Error estimates for lateral and diapycnal fluxes are given in the text and small imbalance in each layer results from choosing a solution where layer residual norms are of $O(1–2 \times 10^6$ m^3 s^{-1}).

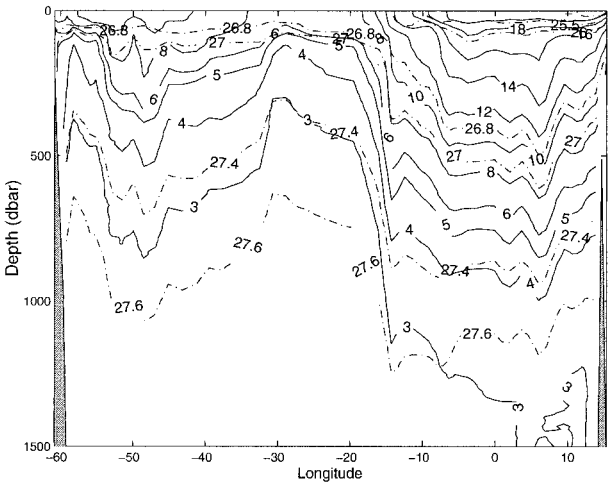

FIG. 7. Temperature (solid: °C) and neutral density (dot-dash: kg m^{-3}) distribution along SAVE4 (47°–30°S). The bounding neutral density surface of thermocline and intermediate water are surface/thermocline $\gamma^n < 26.0$, upper SAMW $26.0 < \gamma^n < 26.8$, lower SAMW $26.8 < \gamma^n < 27.0$, and AAIW $27.0 < \gamma^n < 27.4$.

cesses (warming and freshening of water driven north in the Ekman layer) to SAMW (layers 11–12) (Fig.6). The air–sea processes that convert UCDW to AASW and ultimately to SAMW are partially offset by an interior diapycnal flux of $4 \pm 2 \times 10^6$ m^3 s^{-1} of AAIW into the lightest UCDW (layer 15).

3) RENEWAL AND MODIFICATION

A fundamental question relating to the renewal of the coldest and freshest southwest Atlantic SAMW/AAIW is whether there is a connection between this variety of SAMW/AAIW and that found in the southeast Pacific, or are there two distinct sources of AAIW. McCartney (1977) suggests that southwest Atlantic SAMW/AAIW results from continued deep winter mixing of southeast Pacific SAMW/AAIW through Drake Passage and in the Scotia Sea. Georgi (1979) and Piola and Georgi (1982) find little connection between the coldest southeast Pacific SAMW/AAIW and the even colder, fresher SAMW/AAIW in the southwest Atlantic Ocean. Piola and Georgi (1982) suggest that the cooling and increase in density of SAMW/AAIW between the southeast Pacific and the southwest Atlantic Ocean cannot be solely explained by air–sea heat and freshwater fluxes or cross-frontal mixing of AASW. They support the hypothesis that the coldest Atlantic SAMW/AAIW is formed near the APF, as suggested by Molinelli (1981). A later study by Piola and Gordon (1989) suggests that, indeed, a combination of both air–sea exchange at outcropping SAMW and mixing of AASW near the APF in the region of Burwood Bank (≈54°S and 60°W) can explain the freshening and cooling of lighter varieties of southeast Pacific SAMW/AAIW ($\sigma_\theta = 27.1$) in the southwest Atlantic Ocean. Talley (1996) also discusses a distinction between the formation of SAMW/AAIW in the southeast Pacific and AAIW in the southwest Atlantic Ocean. She suggests that in the southwest Atlantic input from two pools of winter mixed water, south of the SAF and inshore of the Malvinas (Falkland) Current, leads to the formation of southwest Atlantic AAIW. All of the studies emphasize that the renewal of Atlantic SAMW/AAIW occurs in the small region between Drake Passage/Scotia Sea and the southwest Atlantic.

Over the entire region of the Southern Ocean Atlantic sector (Box II), we estimate that air–sea buoyancy fluxes result in the conversion of $8.4 \pm 1 \times 10^6$ m^3 s^{-1} of cold, fresh AASW to lower SAMW (layers 11–12,

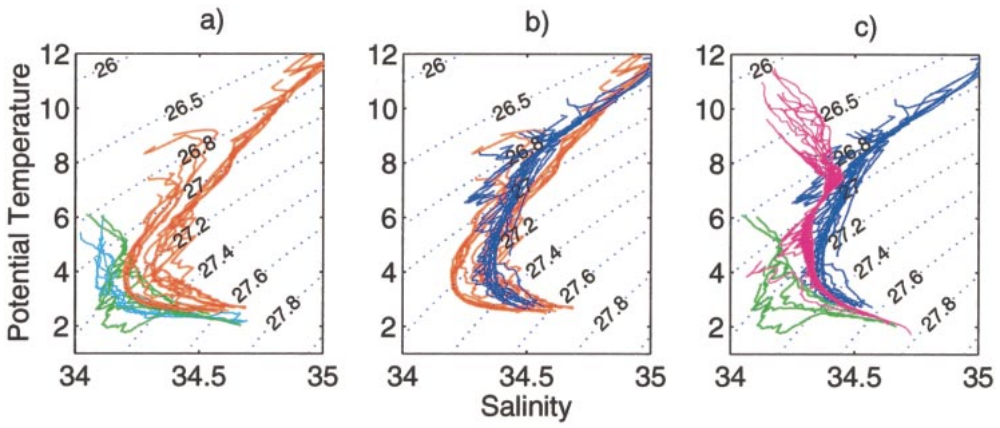

FIG. 8. Comparison of the potential temperature (°C) and salinity (psu) characteristics of SAMW (σ_θ = 26.0–27.0) and AAIW (σ_θ = 27.0–27.4) between the individual sectors of the Southern Ocean. (a) Atlantic: (green) Drake Passage, (light blue) Malvinas Current, and (red) south of Africa; (b) Indian: (red) south of Africa and (blue) south of Australia; (c) Pacific: (blue) south of Australia, (pink) 135°W central Pacific, and (green) Drake Passage. Dashed lines are potential density reference to 0 dbar. Note that the cold, fresh *T*–*S* profiles (σ_θ = 27.2–27.4) in Drake Passage are found in the Antarctic Polar Front zone near 60°S.

γ^n = 26.5–27.0). Although the net production of 8.4 × 10^6 m^3 s^{-1} of SAMW is a basin integral, it is likely that a large portion of this conversion occurs in the southwestern Atlantic region where the SAF extends northward with the Malvinas Current. The northward position of C&F AASW in the southwest Atlantic region results in enhanced air–sea buoyancy fluxes—AASW pushed north in the Ekman layer is warmed and freshened. The addition of C&F AASW and the continued deep winter convection (cooling and freshening) through Drake Passage and the Scotia Sea results in the cooling and freshening of SAMW/AAIW (Fig. 8a; σ_θ = 26.8–27.4). This agrees with the earlier conclusion of Piola and Gordon (1989).

The earlier studies of Georgi (1979) and Piola and Georgi (1982), which show no connection between SAMW/AAIW of the southeast Pacific and southwest Atlantic, are based on the comparison of *T*–*S* properties of SAMW/AAIW within the latitude band 40°–55°S. Unfortunately, in this region of the Southern Ocean the Subantarctic Front reaches its most southerly position in the southeast Pacific at 60°S and attains one of its most northerly positions of 40°S with the northward extension of the Malvinas Current in the southwestern Atlantic (Orsi et al. 1995). SAMW/AAIW between 40° and 50°S in the southeast Pacific has already undergone modification by both air–sea fluxes and mixing with overlying thermocline water as it moves northward away from its formation region and into the Pacific subtropical gyre. At 40°S SAMW/AAIW in the southwest Atlantic has not yet entered the subtropical gyre; it is found just north of the SAF and is therefore subject to renewal by injection of AASW. Georgi (1979) and Piola and Georgi (1982) rightly suggest that there is little connection between SAMW/AAIW at 40°–50°S in the Pacific and SAMW/AAIW at 40°S in the Atlantic but wrongly connect this to little communication between the coldest SAMW/AAIW in the southeast Pacific and southwest Atlantic.

The northward extension of the SAF with the Malvinas Current and associated air–sea buoyancy transformation (heat and freshwater gain) of AASW to lighter SAMW agrees with part of the renewal mechanisms of southwest Atlantic SAMW/AAIW suggested by Talley (1996). However, we find no need for the additional injection of winter-cooled water inland of the Malvinas Current to explain the C&F southwest Atlantic SAMW/AAIW.

Sloyan and Rintoul (2000a) show that interior diapycnal heat and salt fluxes from overlying thermocline water in the subtropical Atlantic (Box I) modify the salinity and temperature of SAMW. Here we have further shown that air–sea fluxes result in the transfer of 6 ± 1 × 10^6 m^3 s^{-1} of W&S thermocline water to SAMW. Much of this modification occurs between the Argentine Basin and the Mid-Atlantic Ridge at 20°W (Fig. 9a; σ_θ = 26.5–27.0). At the western boundary the Brazil Current extends southward, where enhanced heat and freshwater loss converts thermocline water to SAMW. At the Brazil–Malvinas confluence, W&S thermocline water overrides C&F SAMW/AAIW, resulting in interior diapycnal heat and salt fluxes that warm and salinify the newly formed southwest Atlantic mode and intermediate waters. This modification results in a clear distinction between slightly warmer, saltier SAMW (σ_θ = 26.5–27.0) and the underlying AAIW at the mid-Atlantic ridge (Fig. 9a; σ_θ = 27.0–27.4). The increase in temperature and salinity of AAIW between the Argentine Basin and the mid-Atlantic ridge also reflects the effect of mixing in the Brazil–Malvinas confluence.

Schmitz (1995, 1996) describes substantial warming and salinification of SAMW/AAIW between Drake Pas-

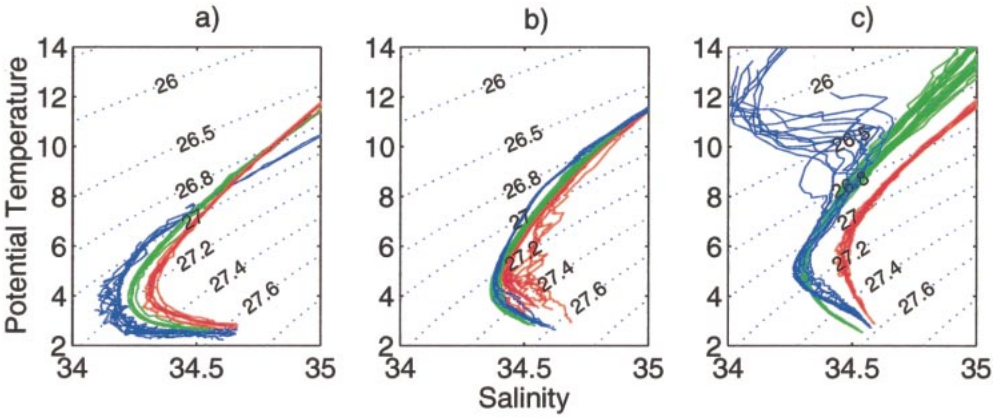

FIG. 9. Comparison of the potential temperature (°C) and salinity (psu) characteristics of SAMW (σ_θ = 26.0–27.0) and AAIW (σ_θ = 27.0–27.4) at 40°–30°S between northward and southward flow in each subtropical basin. (a) Atlantic: (blue) Argentine Basin, (green) mid-Atlantic ridge, and (red) Cape Basin; (b) Indian: (red) Natal Basin, (green) Crozet and Central Basins, and (blue) Perth Basin; (c) Pacific: (red) Tasman Sea and immediately adjacent Kermadec–Tonga Ridge, (green) Southwest Pacific basin and (blue) Chile Basin. Dashed lines are potential density reference to 0 dbar.

sage and 25°W. Mixing between antarctic water and subtropical water at the Brazil–Malvinas confluence has also been previously inferred from the intense finescale features observed there (Georgi 1981). The mixing of low potential vorticity SAMW/AAIW from Drake Passage and the southwest Argentine Basin with higher potential vorticity thermocline and recirculating subtropical modified intermediate water results in the increase in potential vorticity of AAIW and SAMW emanating from the western boundary, as shown by Talley (1996).

Some of the modified W&S SAMW and AAIW is caught in the northward turning of the South Atlantic Current that feeds the Benguela Current (Stramma and Peterson 1989; Peterson and Stramma 1991), while the remainder moves eastward with the ACC south of Africa (Figs. 8a, 9a; σ_θ = 26.5–27.4). The northward export across SAVE4 of $2 \pm 0.5 \times 10^6$ m^3 s^{-1} of thermocline water, $7 \pm 1 \times 10^6$ m^3 s^{-1} of SAMW, and $1 \pm 0.5 \times 10^6$ m^3 s^{-1} of AAIW in the Cape Basin is the major balance of the southward flow of NADW [17×10^6 m^3 s^{-1}; for a discussion of the deep circulation the reader is referred to Sloyan and Rintoul (2000b)]. Figure 9a shows that there is further modification of SAMW and AAIW between the mid-Atlantic ridge and the Cape Basin before the intermediate water moves northward into the subtropical gyre. A detailed description of the circulation path and eventual closure of the North Atlantic thermohaline circulation by SAMW and AAIW is given in section 5.

In the Atlantic, the circulation features that effect the renewal and modification of SAMW/AAIW include: continued deep winter mixing of southeast Pacific SAMW/AAIW in Drake Passage and Scotia Sea; the northward extension of the Malvinas Current along the South American coast; the southward extension of the Brazil Current and its collision with the Malvinas Current, forming the Brazil–Malvinas confluence; and the eastward extension of the SAC. The first two features renew C&F Atlantic SAMW/AAIW and the latter features result in warmer, saltier SAMW and AAIW exiting south of Africa relative to that which enters through Drake Passage and is found in the southwest Atlantic Ocean.

b. Indian sector

1) HORIZONTAL CIRCULATION

At 18°S there is a strong southward transport of 14.4 $\pm$ 1 $\times$ 10^6 m^3 s^{-1} of surface and thermocline water in the Mascarene Basin. Across the remaining basins there is a small northward transport of 2.3 $\pm$ 0.5 $\times$ 10^6 m^3 s^{-1} (Fig. 10). [The lightest water (layer 3) in the Indian sector is denser than the lightest two layers of the model ($\gamma^n \leq 22.5$).] The net southward flux of 12.1 $\pm$ 1 $\times$ 10^6 m^3 s^{-1} of surface and thermocline water (layers 3–9) is dominated by a southward flux of warm surface water (layers 3–4). This includes surface water from the northern Indian Ocean as well as water supplied by the Indonesian Throughflow. The southward flow in these layers is not confined to one particular region but occurs as a shallow flow across the entire Indian Ocean, Mascarene Basin 5.2 $\pm$ 0.5, and remaining basins to the east 8.3 $\pm$ 1 $\times$ 10^6 m^3 s^{-1}. The increased southward flow of surface and thermocline water in the Mascarene basin results from the additional southward flow of 9.2 $\pm$ 0.5 $\times$ 10^6 m^3 s^{-1} of thermocline water (layers 5–9). This southward flow of thermocline water is balanced by a broad northward flow of 10.6 $\pm$ 0.5 $\times$ 10^6 m^3 s^{-1} over the remaining eastern basins. At 18°S there is a northward flux of 9.6 $\pm$ 1.5 $\times$ 10^6 m^3 s^{-1} SAMW and 5.6 $\pm$ 1 $\times$ 10^6 m^3 s^{-1} AAIW in all basins east of the Mascarene Basin. The balancing southward flow is con-

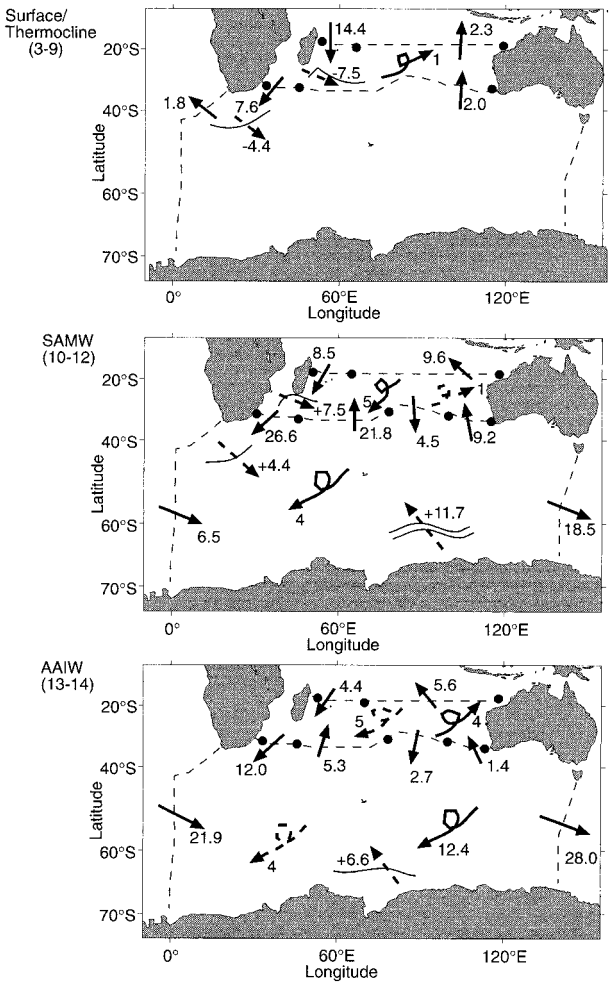

FIG. 10. Lateral and diapycnal volume fluxes ($\times 10^6$ m^3 s^{-1}) in thermocline and intermediate layers for the Indian region (Box IV and V). Lateral fluxes (solid arrows) are shown for part of a section between ●, otherwise total flow across section. Interior diapycnal fluxes are curly arrows, with solid arrow indicating flux across lower interface and dashed arrow flux across upper interface. An upward (downward) diapycnal flux arrow represent upwelling (downwelling) across the interface. Air–sea diapycnal fluxes are dashed arrows angled across the outcropping interface between the water masses, with a positive (negative) value representing an air–sea buoyancy flux gain (loss). Error estimates for lateral and diapycnal fluxes are given in the text and small imbalance in each layer results from choosing a solution where layers' residual norms are of $O(1–2 \times 10^6$ m^3 s$^{-1})$.

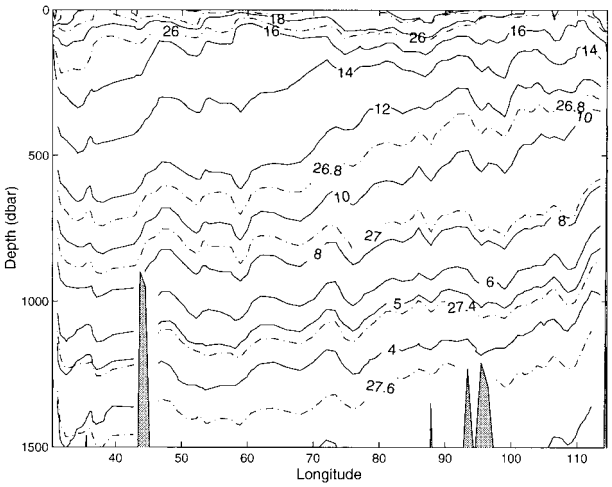

FIG. 11. Temperature (solid: °C) and neutral density surfaces (dot-dash: kg m^{-3}) distribution along Indian 32°S. The bounding neutral density surface of thermocline and intermediate water are surface/thermocline $\gamma^n < 26.0$, upper SAMW $26.0 < \gamma^n < 26.8$, lower SAMW $26.8 < \gamma^n < 27.0$, and AAIW $27.0 < \gamma^n < 27.4$.

fined to the Mascarene Basin in the East Madagascar Current (Fig. 10).

In this model the Mozambique channel between 13° and 26°S is closed. Stramma and Lutjeharms (1997) find a southward transport of 5×10^6 m^3 s^{-1} in the Mozambique Channel and a southward transport of 35×10^6 m^3 s^{-1} east of Madagascar. Sætre and da Silva (1984) suggest that the Mozambique Current is, if at all, only a minor tributary of the Agulhas Current. They even question the concept of a continuous Mozambique Current. Macdonald (1998) resolves the Mozambique channel in her global inverse model and finds no significant flow in the channel. Fu (1986) estimates a southward transport of 6×10^6 m^3 s^{-1} in the Mozambique channel. Although the closure of the Mozambique channel is an undesirable feature of this model, zero mass transport is consistent with previous transport estimates.

Figure 11 shows the temperature and neutral density distribution along the Indian Ocean section at 32°S. At 32°S southward flow of $7.6 \pm 1 \times 10^6$ m^3 s^{-1} of thermocline water (layers 6–9) is concentrated in the Natal Basin (Fig. 10). Across the remaining basins there is a small northward flow of $2.0 \pm 0.5 \times 10^6$ m^3 s^{-1} of lower thermocline water (layers 8–9). SAMW and AAIW enter the subtropical Indian gyre at 32°S via two main routes. In the Crozet and Central Indian Basins, $21.8 \pm 2 \times 10^6$ m^3 s^{-1} of SAMW and $5.3 \pm 1 \times 10^6$ m^3 s^{-1} of AAIW move northward into the subtropical gyre. Further east in the Perth Basin, $9.2 \pm 1 \times 10^6$ m^3 s^{-1} of SAMW and $1.4 \pm 0.5 \times 10^6$ m^3 s^{-1} of AAIW move northward. These northward fluxes are balanced by southward fluxes in the western Natal, Mozambique, and Madagascar Basins (SAMW $26.6 \pm 3 \times 10^6$ m^3 s^{-1}, AAIW $12.0 \pm 1 \times 10^6$ m^3 s^{-1}) and a smaller southward flow over the Ninetyeast Ridge and Broken Plateau (SAMW $4.5 \pm 0.5 \times 10^6$ m^3 s^{-1}, AAIW $2.7 \pm 0.5 \times 10^6$ m^3 s^{-1}) (Fig. 10). The southward transport of intermediate water in the Natal Basin (Agulhas Current) accounts for 75% of the total southward flux of intermediate water. While substantial flows to the north and south occur across 32°S, the net transport of SAMW is $-0.31 \pm 2 \times 10^6$ m^3 s^{-1} (layers 10–12), and AAIW is $-8 \pm 1 \times 10^6$ m^3 s^{-1} (layers 13–14).

The SAMW and AAIW entering the Indian Ocean across 32°S are supplied by the eastward transport of intermediate water in the ACC (Fig. 10). The combined transport of SAMW and AAIW south of Africa is 28.4

$\pm 1 \times 10^6$ m^3 s^{-1}. South of Australia the combined transport increases to $46.50 \pm 1 \times 10^6$ m^3 s^{-1}. The increased volume flux of SAMW and AAIW in the Southern Ocean Indian sector results from significant air–sea and interior diapycnal fluxes that occur across the intermediate layers in both the subtropical and antarctic regions.

The above description of the surface and thermocline and intermediate water circulation in the subtropical Indian Ocean is similar to previous studies (Warren 1981; McCartney 1982; Stramma 1992; Fine 1993). Toole and Warren (1993), Robbins and Toole (1997), and Macdonald (1998) show the same general upper circulation pattern—strong southward flow in the western boundary current and northward flow in the interior—but their net cumulative southward transport of the upper circulation at 32°S is approximately 35×10^6 m^3 s^{-1}, 23×10^6 m^3 s^{-1}, and 24×10^6 m^3 s^{-1}, respectively. This net southward transport results from input of warm Pacific water into the Indian Ocean via the Indonesian Throughflow (6.7×10^6 m^3 s^{-1}, 10×10^6 m^3 s^{-1}, and 10×10^6 m^3 s^{-1}, respectively) and the overturning of bottom and deep water, which move northward in the Indian Ocean at 32°S, upwell, and return as intermediate and thermocline water. Our smaller net southward transport of $14 \pm 2.5 \times 10^6$ m^3 s^{-1} of thermocline and intermediate water is principally the result of the inflow of warm Pacific water via the Indonesian Throughflow, as our deep overturning circulation is essentially balanced below 1500 dbar (Sloyan and Rintoul 2000b).

2) Diapycnal fluxes

Where surface and thermocline layers outcrop in the subtropical Indian Ocean (Box IV), they are exposed to heat and freshwater losses that act to transform large volumes of water to higher density. These air–sea fluxes eventually result in the net transformation of $7.5 \pm 1 \times 10^6$ m^3 s^{-1} of surface and thermocline water (layers 3–9) to SAMW (layers 10–12) (Fig. 10). The net effect of air–sea fluxes in the subtropical Indian Ocean is to transform warm, surface North Indian and Pacific water to denser thermocline water and ultimately SAMW. The interior diapycnal fluxes show an insignificant flux of $1 \pm 2 \times 10^6$ m^3 s^{-1} of SAMW to lighter thermocline layers (Fig. 10). At deeper levels, interior mixing converts $5 \pm 2 \times 10^6$ m^3 s^{-1} of SAMW (layers 10–12) to AAIW (layers 13–14) in the subtropical Indian box. In addition, $4 \pm 2 \times 10^6$ m^3 s^{-1} of UCDW (layers 15–17) is converted to AAIW densities by interior processes. The resulting convergence feeds the export of $-8.0 \pm 1.5 \times 10^6$ m^3 s^{-1} of AAIW from the subtropical Indian Ocean.

Substantial diapycnal fluxes also occur in the Indian sector of the Southern Ocean (Box V). Air–sea buoyancy fluxes result in a transformation of $4.4 \pm 2 \times 10^6$ m^3 s^{-1} of thermocline water to SAMW (layers 10–12) (Fig. 10). As SAMW moves eastward with the Antarctic Circumpolar Current, it is joined by $11.7 \pm 1 \times 10^6$ m^3 s^{-1} of C&F AASW that has been driven north in the Ekman layer and warmed and freshened, resulting in a conversion to SAMW densities.

In the Southern Ocean, AAIW (layers 13–14) moves eastward across the Indian Basin with the ACC. Along its eastward path there are significant inputs: inflow from the subtropical Indian Ocean ($8.0 \pm 1.5 \times 10^6$ m^3 s^{-1}) in this density class, transformation of AASW (6.6×10^6 m^3 s^{-1}) by air–sea buoyancy fluxes, and conversion of SAMW (layer 12) ($4 \pm 2 \times 10^6$ m^3 s^{-1}) to AAIW by interior mixing (Fig. 10). The inflows into AAIW are larger than the loss due to conversion of $12.4 \pm 2 \times 10^6$ m^3 s^{-1} AAIW (layer 14) to UCDW (layers 15–17) by interior mixing, resulting in more AAIW exiting the basin south of Australia than enters south of Africa.

3) Renewal and modification

One of the most notable features of SAMW and AAIW in the subtropical Indian Ocean (Box IV) and Southern Ocean Indian sector (Box V) is the large range of characteristic *T*–*S* properties (Warren 1981; McCartney 1977; Piola and Georgi 1982; Fine 1993; Toole and Warren 1993). Across the Southern Ocean Indian sector, SAMW cools and freshens, and AAIW becomes warmer and saltier (Fig. 8b; SAMW $\sigma_\theta = 26.0$–27.0 and AAIW $\sigma_\theta = 27.0$–27.4). SAMW and AAIW that move northward into the subtropical Indian Ocean are colder and fresher than the intermediate water flowing south in the Agulhas Current (Figs. 11, 9b).

In the subtropical Indian Ocean, unlike the subtropical Atlantic Ocean, the transformation of surface and thermocline water to SAMW by air–sea buoyancy forcing is not compensated by interior diapycnal fluxes from SAMW to thermocline water. Air–sea fluxes convert $7.5 \pm 1 \times 10^6$ m^3 s^{-1} of warm surface and thermocline water to SAMW. Different components of the air–sea flux dominate in different regions of the subtropical Indian Ocean (Sloyan 1997). Evaporation and heat loss beneath the persistent southeast trade winds over the northern portion of the basin result in a transformation of surface and light thermocline water (layers 3–5) to denser thermocline water (layers 6–9). Further cooling of thermocline water in the southern subtropical Indian Ocean is dominated by heat loss over the Agulhas Current.

This study and Sloyan and Rintoul (2000a) show that interior diapycnal fluxes of $5 \pm 2 \times 10^6$ m^3 s^{-1} of SAMW to AAIW further transfer mass, heat, and salt from surface and thermocline water to underlying AAIW. The air–sea transformation and interior diapycnal fluxes result in SAMW and AAIW becoming progressively warmer and saltier as they recirculate in the subtropical gyre (Fig. 9b). The mixing of higher potential vorticity surface and thermocline water with lower potential vorticity SAMW and AAIW also explains the

increase in the potential vorticity of recirculating SAMW and AAIW found at the western boundary (McCartney 1982). SAMW and AAIW that enter in the Crozet and Central Indian Basins are caught in an intense recirculation in the southwest Indian Ocean, while SAMW and AAIW entering the Perth Basin circulate with the basin-scale flow of the subtropical gyre. Import of C&F SAMW and AAIW and export of modified W&S subtropical varieties across 32°S ventilates the lower thermocline of the subtropical Indian Ocean. The return of W&S SAMW and AAIW (and the southward extension of thermocline water in the Agulhas Current and its retroflection) exports heat and salt gained in the subtropical Indian Ocean to the Southern Ocean.

Air–sea and interior diapycnal fluxes modify the characteristic temperature and salinity of SAMW and AAIW as they traverse the Indian sector of the Southern Ocean. Northward fluxes of SAMW in the Crozet, Central, and Perth Basins at 32°S have different *T*–*S* properties (Fig. 9b). W&S varieties of SAMW (σ_θ = 26.5–27.0) are found in the Crozet and Central Indian Basins, and C&F SAMW (σ_θ = 26.5–27.0) moves northward in the Perth Basin. The relatively W&S SAMW of the southwest Indian Ocean is the result of lateral mixing with the ''older'' recirculating SAMW and air–sea fluxes south of Africa. As discussed above, air–sea and interior diapycnal fluxes increase the temperature and salinity of SAMW as it circulates around the subtropical gyre, so that SAMW returning to the south in the Natal Basin is distinctly warmer and saltier (Fig. 9b). In the Southern Indian sector, the Agulhas Current extends southwestward south of Africa and returns eastward (retroflects) at 19°E. Indian Ocean thermocline water (layers 7–9) in the Agulhas current and retroflection loses heat to the atmosphere, which transforms $4.4 \pm 2 \times 10^6$ m^3 s^{-1} of W&S thermocline water to SAMW.

The increases in temperature and salinity of SAMW are gradually removed by the input of $11.7 \pm 1 \times 10^6$ m^3 s^{-1} of AASW across the Polar Front, and by direct cooling, freshening, and homogenization (by winter convection) of this layer where it outcrops. The cooling of the SAMW thermostad is most rapid across the Indian Basin [see Fig. 4 of McCartney (1977)], where the transformation of AASW to SAMW by air–sea fluxes is also greatest. The cooling and freshening of SAMW across the Southern Ocean Indian sector results in the C&F SAMW in the Perth Basin (Fig. 9b).

Fine (1993), using the same Indian 32°S section, finds that warm, lower CFC-11 SAMW moves northward in the Indian Ocean west of 62°S. CFC-11 concentrations and the density of SAMW increases in an eastward direction across the section. These CFC-11 observations are consistent with the modification of SAMW by air–sea fluxes and mixing as it moves eastward with the ACC across the Indian sector.

AAIW, unlike SAMW, is significantly saltier upon leaving the basin south of Australia than when entering the region south of Africa (Fig. 8b; σ_θ = 27.0–27.4. Note that the warmest, saltiest AAIW south of Africa is associated with the Indian–Atlantic interbasin exchange). AAIW leaving the subtropical Indian Ocean in the Natal Basin is much saltier than the AAIW entering across 32°S in the Crozet and Perth Basins, reflecting the interior mixing described above and the input of Red Sea water (Fig. 9b). Salty AAIW carried to the east in the Agulhas extension mixes with the much fresher and slightly cooler AAIW entering from the Atlantic. AAIW properties are further modified by air–sea buoyancy fluxes, which transform $6.6 \pm 1 \times 10^6$ m^3 s^{-1} of AASW to AAIW and an interior diapycnal flux of $4 \pm 2 \times 10^6$ m^3 s^{-1} of SAMW to AAIW. As a result, the AAIW south of Australia has *T*–*S* properties intermediate between the W&S AAIW exported from the subtropical Indian and the C&F variety entering from the Atlantic. The inputs to AAIW in the Southern Ocean more than compensate the interior diapycnal flux of AAIW to UCDW.

Rintoul and Bullister (1999) find that AAIW is defined by a large *T*–*S* range south of Australia. They suggest that AAIW entering the Southern Ocean Pacific sector south of Australia is either a mixture of a number of distinct water masses or is far removed from its source region. In this study we find that the characteristic properties of Southern Ocean Indian sector AAIW result from mixing of C&F Atlantic AAIW with W&S AAIW returning to the Southern Ocean following modification in the subtropical gyre and a small input of AASW.

The air–sea and interior diapycnal fluxes occurring in the Southern Ocean Indian sector and the modification of SAMW and AAIW in the subtropical Indian Ocean sector explain the evolution of the *T*–*S* characteristics across these ocean basins. In particular, there is no renewal of C&F AAIW in the Southern Ocean Indian sector, although there is some input of AASW to AAIW. The input of AASW and eastward transport of Atlantic AAIW only partially erodes the *T*–*S* characteristics of the modified AAIW entering from the subtropics. Conversely, the *T*–*S* characteristics of southwest Indian SAMW (W&S) are steadily eroded by both air–sea fluxes of AASW and deep winter mixing. This supports the early suggestions of McCartney (1977, 1982) that deep winter mixing cools and freshens SAMW as it moves eastward through the Indian sector of the Southern Ocean. However, in addition to deep winter mixing, we also find that cross-front exchange of cold, fresh AASW also plays a significant role in the cooling and freshening trend of SAMW across the ocean basin.

c. Pacific sector

1) HORIZONTAL CIRCULATION

Figure 12 shows the temperature and neutral density distribution along 32° in the Pacific. At 32°S in the Pacific Ocean there is a net northward flux of thermocline water. This occurs principally in the eastern Chile

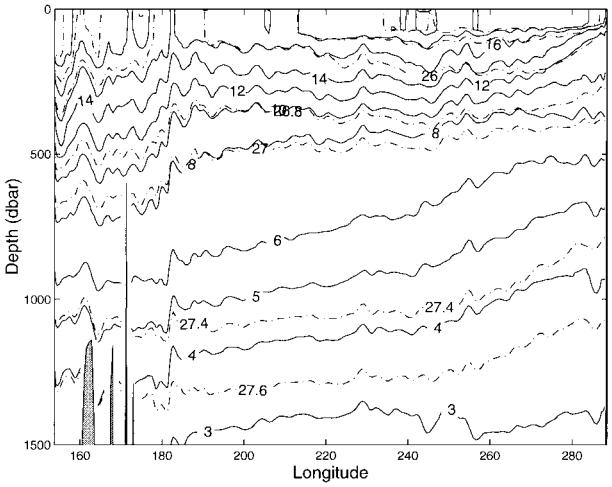

FIG. 12. Temperature (solid: °C) and neutral density surfaces (dot-dash: kg m^{-3}) distribution along Pacific 32°S. The bounding neutral density surface of thermocline and intermediate water are surface/thermocline $\gamma^n < 26.0$, upper SAMW $26.0 < \gamma^n < 26.8$, lower SAMW $26.8 < \gamma^n < 27.0$, and AAIW $27.0 < \gamma^n < 27.4$.

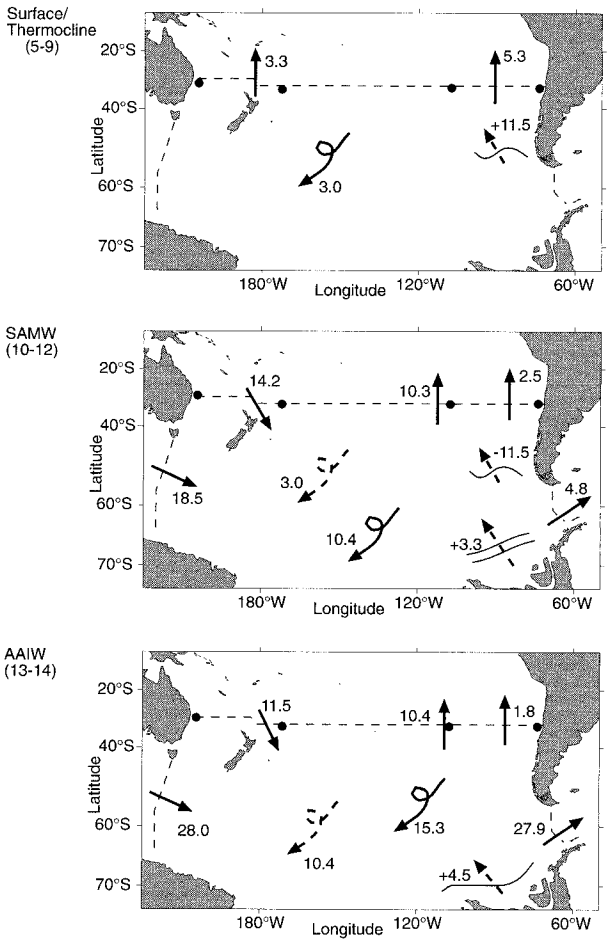

FIG. 13. Lateral and diapycnal volume fluxes ($\times 10^6$ m^3 s^{-1}) in thermocline and intermediate layers for the Pacific region (Box VI). Lateral fluxes (solid arrows) are shown for part of a section between ●, otherwise total flow across section. Interior diapycnal fluxes are curly arrows, with solid arrow indicating flux across lower interface and dashed arrow flux across upper interface. An upward (downward) diapycnal flux arrow represent upwelling (downwelling) across the interface. Air–sea diapycnal fluxes are dashed arrows angled across the outcropping interface between the water masses, with a positive (negative) value representing an air–sea buoyancy flux gain (loss). Error estimates for lateral and diapycnal fluxes are given in the text and small imbalance in each layer results from choosing a solution where layers' residual norms are of $O(1–2 \times 10^6$ m^3 s$^{-1})$.

Basin ($5.3 \pm 0.5 \times 10^6$ m^3 s^{-1}), with a smaller northward flux ($3.3 \pm 0.5 \times 10^6$ m^3 s^{-1}) over the numerous ridges and basins between the Kermadec–Tonga ridge, the Tasman Sea, and in the Southwest Pacific basin (Fig. 13). This description of the thermocline circulation is in agreement with Reid's (1986) adjusted steric heights maps for the sea surface and at 200 dbar.

SAMW and AAIW ($18.5 \pm 0.5 \times 10^6$ m^3 s^{-1} and $28.0 \pm 0.5 \times 10^6$ m^3 s^{-1}, respectively) enter the Pacific sector south of Australia (Fig. 13). In the Southwest Pacific basin, roughly equal amounts of SAMW ($10.3 \pm 0.6 \times 10^6$ m^3 s^{-1}) and AAIW ($10.4 \pm 1 \times 10^6$ m^3 s^{-1}) move northward into the subtropical Pacific (Fig. 13). There is a smaller northward flux of $2.5 \pm 0.4 \times 10^6$ m^3 s^{-1} of SAMW and $1.8 \pm 1 \times 10^6$ m^3 s^{-1} of AAIW in the Chile Basin. The northward flux of SAMW and AAIW in the Southwest Pacific and Chile Basins is balanced by an intense southward flow of subtropical modified intermediate water in the western boundary current adjacent to the Kermadec–Tonga Ridge—$14.2 \pm 0.5 \times 10^6$ m^3 s^{-1} of SAMW and $11.5 \pm 0.2 \times 10^6$ m^3 s^{-1} of AAIW (Fig. 13). Weak net northward flow of intermediate water in the Chile Basin and over the East Pacific rise, stronger northward flow in the Southwest Pacific Basin, and compensating southward flow near and over the Kermadec–Tonga Ridge agrees with Reid's (1986) adjusted steric height maps at 1000 and 1500 dbar. Where the ACC exits the Pacific sector at Drake Passage there is no eastward transport of thermocline water (layers 5–9), a small eastward flux of $4.8 \pm 0.5 \times 10^6$ m^3 s^{-1} of SAMW and $27.9 \pm 0.4 \times 10^6$ m^3 s^{-1} of AAIW.

The circulation in the Pacific sector differs from Macdonald (1998) across the southern subtropical Pacific. Macdonald (1998) has a smaller net northward flux in surface and thermocline water. In her model, the net loss of Pacific water to the Indian Ocean (10×10^6 m^3 s^{-1}) is balanced by the northward flow of thermocline and lower deep water. In this study the net northward transport of thermocline water into the Pacific Ocean at 32°S principally balances the loss of Pacific water to the Indian Ocean via the Indonesian Throughflow (discussed in following section).

2) DIAPYCNAL FLUXES

Buoyancy input by air–sea fluxes in the Pacific sector converts SAMW to thermocline water (Fig. 13). Ad-

jacent to the South American coast, warm and fresh thermocline water extends southward and outcrops. The air–sea conversion of SAMW to thermocline water ($11.5 \pm 1 \times 10^6$ m^3 s^{-1}), driven by warming and freshening of water moving northward in the Ekman layer, occurs there. This transformation is slightly offset by a small net southward flux of $1.4 \pm 1 \times 10^6$ m^3 s^{-1} of SAMW across 32°S and an interior diapycnal flux of $3 \pm 2 \times 10^6$ m^3 s^{-1} of thermocline water to SAMW. The combined interior and air–sea diapycnal fluxes between thermocline and SAMW result in a net transfer of 8×10^6 m^3 s^{-1} of cold, fresh SAMW to lower thermocline water (Fig. 13).

SAMW ($18.5 \pm 0.5 \times 10^6$ m^3 s^{-1}) entering the Pacific south of Australia is cooled and freshened as it moves eastward across the basin by transformation of $3.3 \pm 1 \times 10^6$ m^3 s^{-1} of AASW to SAMW densities, and by oceanic heat loss and freshwater gain as precipitation exceeds evaporation. Interior mixing results in a net conversion of $10.4 \pm 2 \times 10^6$ m^3 s^{-1} of SAMW to AAIW and of 15.3 ± 3 m^3 s^{-1} of AAIW to UCDW, in the Pacific sector (Fig. 13). As a result of exchange with the subtropical Pacific, and diapycnal fluxes due to interior mixing and air–sea transformation, the Pacific as a whole imports 13.7×10^6 m^3 s^{-1} of SAMW (the difference between 18.5×10^6 m^3 s^{-1} entering south of Australia and 4.8×10^6 m^3 s^{-1} leaving through Drake Passage). The net transport of AAIW is similar at the two meridional lines bounding the basin, but substantial modification of the *T*–*S* properties of AAIW occurs across the basin as a result of diapycnal fluxes (discussed below).

3) Renewal and modification

In the Pacific, C&F SAMW and AAIW ($\sigma_\theta = 26.0$–27.4) enter the subtropics in the eastern part of the Southwest Pacific Basin and in the Chile Basin (Figs. 12, 13, 9c). In a similar fashion to the Indian Basin, the northward flow of intermediate waters is balanced by a concentrated southward return flow in the western boundary current of subtropical modified W&S mode and intermediate water (Fig. 9c; $\sigma_\theta = 26.0$–27.4).

Figure 8c shows the *T*–*S* changes in SAMW and AAIW across the Pacific sector of the Southern Ocean. To better reveal the evolution of *T*–*S* characteristics across the basin, the sections south of Australia and in Drake Passage are supplemented by a WOCE section at 135.5°W (P16) in the central Pacific.

In contrast to the situation south of Africa, no increase in temperature and salinity of SAMW is observed at the transition from the Indian to the Pacific Oceans; indeed, maps of, for example, temperature and salinity at 200 m (Gordon and Molinelli 1982) suggest a sudden jump to cooler, fresher SAMW southeast of New Zealand [Fig. 8c; see also McCartney (1977)]. This is likely due in part to the lack of interaction between W&S thermocline water carried by the weak southward extension of the East Australian Current and the C&F water of the ACC. Perhaps more importantly, Rintoul and Bullister (1999) emphasize the fact that most of the SAMW/AAIW found north of the ACC at 140°E recirculates south of Australia, rather than being carried to the east to enter the Pacific Ocean; the warmer SAMW of the southeast Indian Ocean and southwest Pacific Ocean appear to be two largely independent pools blocked by the Campbell Plateau (164°E), and the jump in SAMW properties is not an indicator of intense air–sea fluxes converting warm, salty to cold, fresh SAMW but of a shift in dominance of colder, fresh SAMW east of the topographic restriction.

Between southern Australia and 135°W there is also some freshening of the lightest AAIW (layer 13 $\sigma_\theta = 27.0$–27.2) due to cross-frontal exchange of C&F AASW. As a result, the salinity minimum shifts to cooler, fresher, and lighter water across the basin. Note, however, that the densest AAIW (layer 14; $\sigma_\theta = 27.2$–27.4) has similar *T*–*S* properties south of Australia (WOCE SR3) and at 135°W (WOCE P16). This indicates that the relatively dense water that forms the salinity minimum core south of Australia is only slightly modified by diapycnal processes during its transit of the Pacific to 135°W.

Continued cooling and freshening of SAMW east of the Campbell Plateau occurs from input of $3.3 \pm 1 \times 10^6$ m^3 s^{-1} of C&F AASW across the Polar Front and cooling and freshening by air–sea fluxes at the layer outcrop. The shift to a colder, fresher variety of SAMW east of the Campbell Plateau, and input of C&F AASW and winter mixing in the Southern Ocean Indian sector has already removed much of the buoyancy of SAMW; further buoyancy forcing drives deep mixing that is efficient in converting $10.4 \pm 2 \times 10^6$ m^3 s^{-1} of SAMW to slightly denser AAIW. The southward movement of the ACC in the Pacific–Antarctic Basin of the southeast Pacific allows AAIW to outcrop, and $4.5 \pm 1 \times 10^6$ m^3 s^{-1} of AASW is transformed directly to AAIW.

In an early study, Molinelli (1981) finds that 6×10^6 m^3 s^{-1} of SAMW and 5×10^6 m^3 s^{-1} of AASW contribute to the renewal of southeast Pacific AAIW. In this study we find a contribution of 10×10^6 m^3 s^{-1} of SAMW and 5×10^6 m^3 s^{-1} of AASW to AAIW in the Pacific sector.

The dramatic changes in water properties on the salinity minimum core layer between the Indian and Pacific Basins [see, e.g., the plates in Gordon and Molinelli (1982)] result from the formation of a new, lighter water mass in the southeast Pacific, of even lower salinity, which overrides the denser AAIW imported from the Indian Ocean. The particularly C&F AAIW of the southeast Pacific is formed from SAMW that has been cooled and freshened across the basin, as proposed by McCartney (1982). However, the cooling and freshening is not solely due to air–sea exchange with outcropping SAMW, as suggested by McCartney (1982); cross-fron-

tal transport and transformation of AASW plays a significant role.

d. Circumpolar summary

Summing over all three sectors, there is a net input of 23.4×10^6 and 11.1×10^6 m^3 s^{-1} of AASW to SAMW and AAIW, respectively. The largest input of AASW to SAMW and AAIW ($11.7 \pm 1 \times 10^6$ and $6.6 \pm 1 \times 10^6$ m^3 s^{-1}, respectively) occurs in the Indian sector. The cross-frontal exchange of AASW to SAMW, and air–sea exchange where SAMW outcrops, erode the W&S southwest Indian Ocean SAMW characteristics as SAMW moves eastward through the region. The exchange of AASW and deep winter mixing increases the density of SAMW and begins the process by which further cooling and conversion of AASW ($3.3 \pm 1 \times 10^6$ m^3 s^{-1} to SAMW and $4.5 \pm 1 \times 10^6$ m^3 s^{-1} to AAIW) in the Pacific sector results in cold, fresh SAMW, which is converted to slightly higher density AAIW. The southeast Pacific SAMW/AAIW is carried into the southwest Atlantic where further winter cooling and conversion of AASW ($8.4 \pm 1 \times 10^6$ m^3 s^{-1}) produces the coldest, freshest SAMW/AAIW.

In this study, the buoyancy transformations and air–sea exchange acting on SAMW in the Southern Ocean are distributed to AAIW by interior mixing. In this model, ''interior'' means everything below the sea surface, including horizontal mixing across the nearly vertical isopycnals in the mixed layer. Marshall et al. (1999) find that vertical and lateral diffusive fluxes reconcile air–sea transformation and mixed layer subduction rates. At high latitudes (i.e., Southern Ocean) they find that lateral diffusion between different water classes in the mixed layer is particularly important in this reconciliation. Nurser et al. (1999) find a similar balance between the air–sea transformation and diffusive mixing in particular water masses in the North Atlantic. Although our model does not explicitly include a mixed layer model, we suggest that much of the ''interior'' mixing of SAMW to AAIW occurs in the mixed layer. This mixing redistributes the large effect of direct air–sea forcing on SAMW to AAIW and results in a net subduction of both SAMW and AAIW into the ocean interior.

As suggested by McCartney (1977), we find that the air–sea exchange at outcropping SAMW results in the renewal of cold, fresh AAIW in the southeast Pacific and southwest Atlantic. However, we also find that the cooling and freshening is not solely due to air–sea exchange at the outcropping SAMW; cross-frontal transport and transformation of AASW also play an important role. Molinelli (1981) also suggests the importance of AASW in the renewal of cold, fresh AAIW. But he proposes that AAIW is formed by isopycnal exchange with AASW across the Polar Front. In this study we find that AASW is transformed, principally to SAMW densities, by northward Ekman drift that is warmed and freshened across the Polar Front, a diapycnal exchange.

As SAMW and AAIW circulate in the Antarctic Circumpolar Current and the subtropical gyres, significant changes to their characteristic temperature and salinity occur. C&F mode and intermediate water ventilating the subtropical gyres are balanced by returning W&S mode and intermediate water. McCartney (1977, 1982) and Piola and Georgi (1982) note that the temperature and salinity of SAMW and AAIW change abruptly across the transition between each basin of the Southern Ocean, particularly between the Southern Ocean Atlantic and Indian sectors. These abrupt changes in *T*–*S* characteristics result from enhanced exchange (air–sea and interior) between subtropical thermocline and recirculating SAMW and AAIW water and C&F SAMW and AAIW in the ACC. Notable regions of enhanced mixing include the Brazil–Malvinas confluence, and the southwestward extension and retroflection of the Agulhas Current south of Africa. Away from these transition regions, more gradual *T*–*S* modifications of SAMW and AAIW result from the input of AASW and air–sea exchange at layer outcrops.

Balancing the transformation of AASW to SAMW and AAIW is an interior diapycnal flux of 31.7×10^6 m^3 s^{-1} of AAIW to UCDW. (UCDW, in turn, outcrops south of the Polar Front where air–sea fluxes modify its property characteristics to that of AASW, and convert AASW to SAMW/AAIW.) In a steady-state ocean, this compensation must be exact when the global extent of an isopycnal layer is considered (Tziperman 1988). Our results suggest that most of this compensation occurs within the Southern Ocean itself. Evidence of large-scale mixing in the Southern Ocean is limited, but a recent study by Polzin and Firing (1997) finds enhanced mixing below 1000 m in the Southern Ocean Indian sector over that seen in the subtropical Indian Ocean.

The input of slightly higher oxygen AAIW to UCDW is also consistent with small increases observed in the oxygen concentration between Indian Deep Water at 32°S (oxygen concentration of ≤ 175 μmol kg^{-1}) and UCDW south of Australia (oxygen concentration ≤ 200 μmol kg^{-1}), and between Pacific Deep Water at 32°S (oxygen concentration of ≤ 150 μmol kg^{-1}) and UCDW in Drake Passage (≤ 175 μmol kg^{-1}). Importantly, the mass balance between cold, fresh AASW and slightly warmer, saltier AAIW provides a mechanism by which heat and salt gained by AAIW along its circulation route (both circumpolarly and in the subtropics) through diapycnal mixing is transported southward across the Polar Front zone. The overall effect is the exchange of freshwater and heat between the subtropical and subpolar regions and the high polar southern latitudes.

5. SAMW and AAIW components of the thermohaline circulation

The Southern Ocean plays an important role in the global thermohaline circulation and interbasin exchange as it provides a conduit by which Atlantic, Indian, and

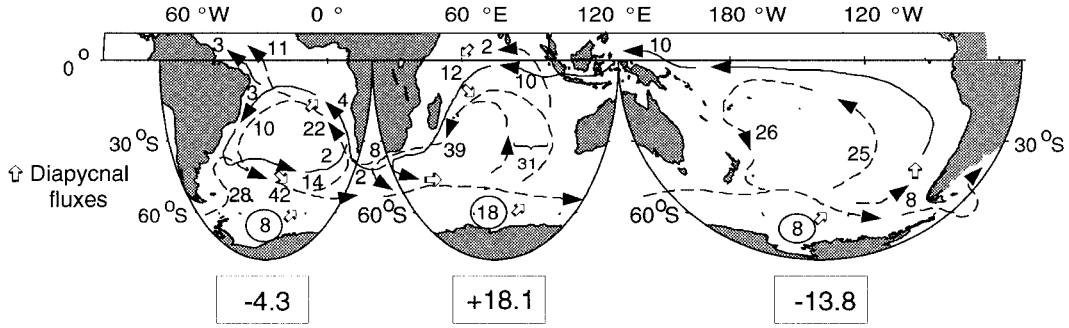

FIG. 14. Upper-layer volume fluxes ($\times 10^6$ m^3 s^{-1}) of thermocline (layers 1–9: solid line) and intermediate water (SAMW/AAIW layers 10–14: dashed line) involved in the global thermohaline circulation, closure of the North Atlantic thermohaline circulation and Pacific–Indian interbasin exchange. The open arrows represent air–sea and interior diapycnal fluxes. Circled numbers in each of the Southern Ocean sections represent conversion of UCDW to SAMW and AAIW. Fluxes in boxes are the net convergence (+ve) or divergence (−ve) of SAMW/AAIW in that sector of the Southern Ocean due to meridional and diapycnal fluxes; mass is conserved by a compensating divergence in zonal transport of the ACC.

Pacific Ocean water masses are freely exchanged and/or modified. SAMW and AAIW are sandwiched between overlying thermocline and underlying deep water and they circulate in both the Southern Ocean and all adjacent subtropical oceans. Therefore, SAMW and AAIW must be active members in the closure of the deep and thermocline circulation in the Southern Ocean and/or the adjacent subtropical oceans.

In the following section the influences of SAMW and AAIW in the global thermohaline circulations will be shown. First, we begin with the deep thermohaline circulation and finally the Indonesian Throughflow.

a. Deep-to-intermediate circulation

The most widely recognized part of the deep overturning circulation is NADW. NADW sinks in the northern Atlantic Ocean, flows southwards into the South Atlantic, and is eventually entrained into Lower Circumpolar Deep Water in the Southern Ocean (Sloyan and Rintoul 2000b). The NADW exported from the Atlantic into the southern oceans is compensated by northward flow of intermediate and thermocline water in the Atlantic Ocean. However, although we know that southward NADW is balanced by northward transport of thermocline and intermediate water, there is considerable debate about the mixing mechanism that converts NADW to thermocline and intermediate water, and where this occurs (Gordon 1986; Rintoul 1991; Schmitz 1996; Döös and Coward 1997).

Sloyan and Rintoul (2000b) show that bottom and lower deep water (including NADW) entering the Indian and Pacific subtropical oceans are balanced by southward flow of upper deep water (Fig. 5). The return of upper deep water to the Southern Ocean represents the first step in the closure of the NADW thermohaline circulation. The returning upper deep water upwells south of the Antarctic Polar Front, and air–sea fluxes result in *T–S* characteristics of AASW and conversion to lighter SAMW and AAIW (Sloyan and Rintoul 2000b). The upwelling of upper deep water and conversion to intermediate water by air–sea fluxes provide the ''upward'' limb of the NADW cell.

Schmitz (1996) also converts upper deep water to intermediate water in the Southern Ocean. However, he shows this only as a balance between NADW and intermediate water. In this study we show that the 10×10^6 m^3 s^{-1} of intermediate water that compensates the NADW is a minor component of a larger (34×10^6 m^3 s^{-1}) deep to intermediate water (DW–IW) circulation.

The DW–IW cell connects the deep circulation, including NADW, to the upper intermediate circulation (Fig. 14). The conversion of AASW to SAMW/AAIW and deep winter mixing renews C&F SAMW/AAIW. New SAMW/AAIW moves northward into the subtropical gyres—22×10^6 m^3 s^{-1} Atlantic, 31×10^6 m^3 s^{-1} Indian, and 25×10^6 m^3 s^{-1} Pacific—and is essentially balanced by southward return flow of subtropical modified mode and intermediate water and NADW.

BALANCING THE NADW: PATHWAYS AND MODIFICATION OF SAMW/AAIW

Although intermediate water flows northward in the eastern Atlantic to close the NADW thermohaline circulation, there is still uncertainty about the circulation path of the intermediate water before it moves northward into the Atlantic Ocean. This study and studies by Rintoul (1991), Gordon et al. (1992), Macdonald (1993), and Schmitz (1995, 1996) suggest that the North Atlantic thermohaline circulation is closed primarily by intermediate water that enters the Atlantic through Drake Passage, the ''cold water path,'' while Gordon (1986) and Saunders and King (1995) suggest that NADW is closed by upwelling of deep water to thermocline water in the Pacific and Indian that returns to the Atlantic Ocean south of Africa (via the Indonesian Throughflow), the ''warm water path.''

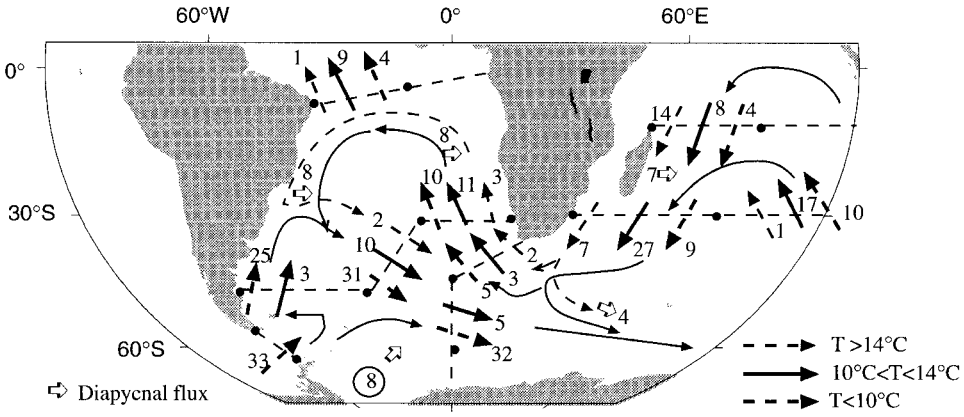

FIG. 15. Mass flux ($\times 10^6$ m^3 s^{-1}) of layers above 1500 dbar involved in the Atlantic–Indian interbasin circulation. The water layers are thermocline temperature $T > 14$°C, Upper Intermediate (SAMW) $10° < T < 14$°C, and Lower Intermediate (AAIW) $T > 10$°C. Lateral fluxes are shown for part of a section between ●. Also given are the diapycnal fluxes between thermocline and intermediate water classes and the underlying circulation pattern; thermocline dashed; and intermediate (both temperature classes) solid. Circled number in the Southern Ocean Atlantic sector represents the conversion of UCDW to SAMW and AAIW. Inflows/outflows across lower intermediate layers do not balance as diapycnal fluxes across the intermediate–deep interface is not shown.

Stramma and Peterson (1990) suggest that the SAC is the primary source of the Benguela Current. Gordon et al. (1992) conclude, on the basis of differences in the equilibrium ratio of chlorofluoromethane 11 (CFM-11) to chlorofluoromethane 12 (CFM-12) between the Benguela Current and the SAC, that the SAC does not flow directly into the Benguela Current. They determine that intermediate water in the Benguela Current is a mixture of South Atlantic and Indian Ocean water.

A three-layer upper Atlantic–Indian circulation derived from this study is shown in Fig. 15. Following Gordon et al. (1992), the water column is divided into three layers: water warmer than 14°C (surface and thermocline water layers 1–9 or 10; γ^n (σ_θ) = surface–26.0 or 26.5), water between 14° and 10°C (upper SAMW layers 10–11 or 12; γ^n (σ_θ) = 26.0–26.5 or 27.0), and water colder than 10°C (lower SAMW and AAIW layers 12–14; $\gamma^n(\sigma_\theta)$ = 27.0–27.4) but shallower than 1500 dbar. (The difference in fluxes between Fig. 15 and earlier figures result from the slightly different grouping of model layers into water classes based on temperature rather than density, as was previously used. In Fig. 15, the diapycnal fluxes across the lower interface (layer 14, not shown) balance the inflow/outflow in intermediate layers.)

Cool SAMW/AAIW enters the Southern Ocean Atlantic sector and moves northward adjacent to the South American coast with the Malvinas Current (Fig. 15). Between 38° and 33°S it meets the southward Brazil Current, forming the Brazil–Malvinas confluence, which moves eastward across the Atlantic as the SAC. At the Brazil–Malvinas confluence, C&F SAMW/AAIW is capped by less dense surface and thermocline water in the Brazil Current. As discussed, capping of SAMW/AAIW by W&S thermocline water and the juxtaposition of subtropical modified mode and intermediate waters enhances air–sea and interior diapycnal and isopycnal fluxes resulting in modified (W&S) SAMW and AAIW, which is transported southeastward over the mid-Atlantic ridge (Fig. 9a).

The mass fluxes in the three temperature classes south of Africa are shown for stations between 0° and 20°E and the remaining stations along 0°, north of the SAF. The stations between 0° and 20°E are west of the mean position (16°–20°E) of the Agulhas retroflection (Lutjeharms and Van Ballegooyen 1988). Therefore, it is appropriate to assume that most of the westward flow south of Africa enters the Atlantic Ocean in the Benguela Current. The largest westward transport in the three temperature classes occurs in the lower SAMW and AAIW stratum: $2 \pm 0.3 \times 10^6$ m^3 s^{-1} of warm surface and thermocline water, $3 \pm 1 \times 10^6$ m^3 s^{-1} of upper SAMW, and $5 \pm 0.5 \times 10^6$ m^3 s^{-1} of lower SAMW and AAIW.

The NADW thermohaline circulation is closed in the eastern basin of SAVE4 by the northward transport of thermocline, mode, and intermediate water in the Benguela Current. The northward transport of $3 \pm 0.5 \times 10^6$ m^3 s^{-1} of thermocline water in the Benguela Current results from a combination of thermocline water that moves eastward with the SAC across the mid-Atlantic ridge and westward transport, south of Africa, of Indian Ocean thermocline water (Fig. 15). Upper SAMW ($10°C < T < 14°C$) moving into the subtropical Atlantic in the Benguela Current is dominated by modified W&S upper SAMW that flows eastward over the mid-Atlantic ridge and northward with the SAC, while lower SAMW and AAIW moving northward has equal contributions from the SAC and Indian Ocean. The closure of the NADW thermohaline circulation by a mixture of thermocline water, SAMW, and AAIW that are modified in

the Brazil–Malvinas confluence, along the SAC and in the southwest Indian Ocean, results in *T–S* profiles in the Cape Basin that lie between those at the mid-Atlantic ridge and immediately adjacent to southern Africa (Fig. 9). At SAVE2 only a small amount of thermocline water moves northward in the North Atlantic, while the major balance of NADW is achieved through northward transport of $9 \pm 1 \times 10^6$ m^3 s^{-1} of upper SAMW and a smaller transport of $4 \pm 1.5 \times 10^6$ m^3 s^{-1} of lower SAMW and AAIW (Fig. 15).

The inverse model provides us with an estimate of the net leakage of Indian thermocline and modified SAMW and AAIW to the Atlantic Ocean. Much of this exchange is thought to be achieved by Agulhas eddies (de Ruitjer et al. 1999). Agulhas eddies are shed from the Agulhas Current at irregular intervals, with an average frequency of six per year (de Ruitjer et al. 1999). The property fluxes associated with each eddy also vary considerably: mass 0.4–1.5 $\times 10^6$ m^3 s^{-1}, heat 1.0–2.5 $\times 10^{-3}$ PW, and salt 0.15–6.3 $\times 10^6$ kg s^{-1}. The section across the Benguela Current does contain a warm eddy between 250 and 1000 dbar at 5°E (Fig. 7, third panel). The influence of this eddy is a component of the total northward transport of warm, salty SAMW and AAIW in the Benguela Current. Agulhas eddies or the leakage of Indian Ocean water to the Atlantic Ocean does not provide unequivocal evidence for the ''warm water'' closure route of NADW. As shown, water that leaks from the Indian Ocean to the Atlantic can be derived from Drake Passage. Intermediate water undergoes considerable air–sea transformation and interior diapycnal fluxes along its path from Drake Passage to southern Africa and is also caught in the intense circulation in the southwest Indian Ocean. Mixing along this route results in a warming and salinification of SAMW and AAIW that enters through Drake Passage before it moves northward with the Benguela Current.

A comparison of the upper water closure of NADW from this study (Fig. 14) to the conceptual cartoons of Gordon et al. (1992) shows some similarities, while comparisons with the interbasin exchange of Schmitz (1996) shows some disagreement. [Combining the two densest layers of Schmitz's (1996) Fig. II-159 results in a three-layer circulation that is equivalent to the layer description defined in this study and Gordon et al. (1992).] Gordon et al. (1992) finds that NADW is balanced by thermocline water, SAMW, and AAIW. The thermocline, SAMW, and AAIW are fed from northward flow of the SAC and westward flow south of Africa. However, they find a larger input of thermocline and upper SAMW south of Africa (10×10^6 m^3 s^{-1}) and a smaller input of these water masses directly from the SAC than found in this study. In Schmitz's (1996, his Fig. II-159) interbasin circulation, NADW is equally balanced by 1) SAMW and AAIW that originates as eastward flow through Drake Passage, is modified in the Brazil–Malvinas confluence, and flows northward with the SAC, and 2) westward flow south of Africa of warm Indonesian Throughflow water and a portion of upwelling deep water. In Schmitz's interbasin exchange there is no buoyancy transformation (heat and freshwater loss) of Indian Ocean surface and thermocline water to SAMW. Schmitz's scheme also requires a large conversion of Circumpolar Deep Water to surface water in the Indian and Pacific, which is inconsistent with middepth southward flow of upper deep water (Toggweiler and Samuels 1993; Sloyan and Rintoul 2000b).

The Atlantic as a whole exchanges intermediate water for deep water (Fig. 14). Rintoul (1991) reached a similar conclusion, and noted that some mechanism must convert C&F Drake Passage water to the W&S (and somewhat lighter) water flowing north in the upper limb of the NADW overturning circulation. However, his model did not explicitly represent the processes responsible for the water mass conversion. Here we have shown how air–sea fluxes and interior mixing drive the significant water mass changes observed between Drake Passage, the subtropical Atlantic, and south of Africa, and produce the W&S SAMW and AAIW that close the NADW thermohaline circulation.

b. Indonesian Throughflow

Our results suggest that the Indonesian Throughflow is part of an Indian–Pacific circulation restricted to the upper layers of the ocean (Fig. 14). To complete the circum-Australia circulation, warm Pacific water must be converted to SAMW in the subtropical Indian Ocean (Box IV) and Southern Ocean Indian sector (Box V) to feed the excess leaving the basin in this density class south of Australia, and SAMW must in turn be converted to thermocline water in the Pacific. We show how air–sea fluxes and the transformations they drive accomplish the water mass modifications required to complete this cell. Indonesian Throughflow water is converted to thermocline water in the Indian subtropical gyre, and further transformed to SAMW by strong cooling in the Agulhas Current and its southward extension. As SAMW crosses the Indian sector from west to east, it is cooled and freshened by exchange of AASW across the Polar Front and air–sea exchange at outcropping SAMW. In the Pacific sector [especially the Chile Basin, as speculated by Schmitz (1996)], air–sea fluxes convert SAMW to cool, fresh thermocline water that is transported northward into the Pacific Ocean, balancing the Pacific–Indian Ocean leakage. Closure of the Indonesian Throughflow by upper water via a circum-Australia route conflicts with the notion of a throughflow fed by upwelling of deep water in the subtropical basins associated with the North Atlantic Deep Water overturning circulation (Gordon 1986).

Schmitz (1996) also suggests that the Indonesian Throughflow is fed by northward flow of lower SAMW and AAIW across 30°S in the Pacific Ocean. However, he shows no air–sea buoyancy loss over surface and thermocline water in the subtropical Indian Ocean, and

Indian Throughflow water eventually moves westward, south of Africa, balancing NADW.

Macdonald (1998) and Macdonald and Wunsch (1996) also suggest that the throughflow is part of an Indian–Pacific circulation that is largely independent of the North Atlantic Deep Water overturning circulation. However, there is an important difference between the depth interval involved in the circulation between their study and ours. Macdonald (1998) and Macdonald and Wunsch (1996) close the Indian–Pacific circulation by an equal northward transport of deep and upper water into the Pacific. The deep water upwells into the thermocline in the north Pacific, where air–sea heat fluxes complete the conversion to warm surface water. The warm surface water is transported into the Indian Ocean via the Indonesian Throughflow. In this study, the Indonesian Throughflow is completely balanced by northward flow of lower thermocline water (layers 8 and 9). The implied conversion of deep water to thermocline water in the North Pacific Ocean as suggested by Macdonald (1998) is inconsistent with the deep circulation of this model (Sloyan and Rintoul 2000b) and earlier studies by Wunsch et al. (1983), Toggweiler and Samuels (1993), and Wijffels et al. (1996).

6. Conclusions

A box inverse model is used to determine the circulation of SAMW and AAIW in the Southern Hemisphere oceans, including diapycnal fluxes due to interior mixing and water mass transformation driven by air–sea buoyancy fluxes. The fluxes due to interior mixing and water mass transformation are significant terms in the budgets and circulation of SAMW and AAIW. A consistent description of the circulation of SAMW and AAIW must include an adequate representation of both diapycnal fluxes.

As suggested by McCartney (1977), we find that the air–sea exchange at outcropping SAMW results in the renewal of cold, fresh AAIW in the southeast Pacific and southwest Atlantic. However, we also find that the cooling and freshening is not solely due to air–sea exchange at the outcropping SAMW; cross-frontal transport and transformation of 34×10^6 m^3 s^{-1} of AASW also play an important role. The cross-frontal exchange of AASW to SAMW and air–sea exchange with outcropping SAMW erode the warm, salty southwest Indian Ocean SAMW characteristics as SAMW moves eastward through the region. The exchange of AASW and deep winter mixing increase the density of SAMW and begin the process by which further cooling and exchange of AASW in the Pacific sector results in cold, fresh SAMW that is converted to slightly higher density AAIW. The southeast Pacific SAMW/AAIW is carried into the southwest Atlantic where further air–sea exchange at outcropping SAMW and exchange of AASW result in the coldest, freshest SAMW/AAIW.

Ventilation of the lower thermocline of the subtropical gyres is accomplished by equatorward flow of ''new'' SAMW and AAIW. A nearly equal amount of ''old'' modified SAMW and AAIW returns poleward in each basin. While the net meridional transport across 30°–40°S in these layers is small when integrated around the globe, the gross exchange is approximately 80×10^6 m^3 s^{-1}. Given the vigor of this exchange, even small differences in properties (temperature, salinity, oxygen) between the equatorial and poleward flow can result in significant meridional transports.

In the Southern Ocean, an interior diapycnal flux of 31.7×10^6 m^3 s^{-1} of AAIW to UCDW balances the air–sea transformation of AASW to SAMW and AAIW. The compensation by slightly warmer, saltier AAIW for cold, fresh AASW results in a transfer of heat and salt, which are gained by AAIW along its circumpolar and subtropical circulation path through diapycnal mixing, southward across the Polar Front zone.

That deep water is converted to intermediate water in the Southern Ocean, rather than uniform interior upwelling, means that the intermediate and deep circulation are largely isolated from each other in the subtropics. This is contrary to numerous conceptual models of the deep circulation (e.g., Stommel and Arons 1960; Munk 1966; Gordon 1986).

SAMW and AAIW are central players in the large-scale interbasin circulation cells associated with the NADW overturning and Indonesian Throughflow. The North Atlantic thermohaline circulation is closed by intermediate water that enters through Drake Passage. Before moving northward along the eastern boundary in the Benguela Current, intermediate water undergoes significant modification by air–sea buoyancy transformation and interior diapycnal fluxes at the Brazil–Malvinas confluence, along the eastward extension of the South Atlantic Current, and during a sojourn into the southwest Indian Ocean. The modification processes in the Atlantic sector produce warm, salty SAMW, which makes the major contribution to the northward limb of the NADW cell, while equal amounts of Atlantic modified and southwest Indian modified lower SAMW and AAIW supply the rest of the northward flow.

The Indonesian Throughflow is found to be part of a circum-Australia circulation. Warm, surface Indonesian Throughflow water is converted to thermocline water in the subtropical Indian Ocean and eventually to SAMW by intensive heat loss over the Agulhas Current and its southward extension and retroflection. This conversion to SAMW feeds the excess water leaving the Southern Ocean in this density class south of Australia. In the Southern Ocean Pacific sector SAMW is converted to thermocline water by air–sea buoyancy fluxes and is transported northward across 32°S into the Pacific Ocean.

This study has shown that diapycnal transports driven by air–sea fluxes and interior mixing are a significant part of the circulation, renewal, and modification of SAMW and AAIW in the Southern Hemisphere oceans.

Improved air–sea climatologies and independent estimates of diapycnal mixing along with the use of the repeat hydrographic data in a suitably designed inverse model will provide improved estimates of these fluxes, and their variability.

Acknowledgments. The majority of this work was done while B. Sloyan was a student at the Institute of Antarctic and Southern Ocean Studies, University of Tasmania, Hobart, Australia. We thank Phil Morgan for writing the Dobox code. The mid-Pacific (P16) *T–S* data were obtained from the WOCE hydrographic office. This work is supported by Environment Australia through the National Greenhouse Research Program. This study contributes to the World Ocean Circulation Experiment.

REFERENCES

Barnier, B., L. Siefridt, and P. Marchesiello, 1995: Thermal forcing for a Global Ocean Circulation using a three year climatology of ECMWF analysis. *J. Mar. Syst.,* **6,** 363–380.

Baumgartner, A., and E. Reichel, 1975: *The World Water Balance.* Elsevier, 179 pp.

Budd, W. F., P. A. Reid, and L. J. Minty, 1995: Antarctic moisture flux and net accumulation from global atmospheric analyses. *Ann. Glaciol.,* **21,** 149–156.

Coachman, L., and K. Aagaard, 1988: Transport through Bering Strait: Annual and interannual variability. *J. Geophys. Res.,* **93,** 15 535–15 539.

da Silva, A. M., C. C. Young, and S. Levitus, 1994: *Atlas of Surface Marine Data 1994. Vol. 1: Algorithms and Procedures*, NOAA/NESDIS Tech. Rep. 6, 83 pp.

Deacon, G. E. R., 1937: *The Hydrology of the Southern Ocean.* Vol. 15, Cambridge University Press, 3–12.

de Ruitjer, W. P. M., A. Biastoch, J. R. E. Drijfhout, S. S. Lutjeharms, R. P. Matano, T. Pichevin, P. J. van Leeu Wen, and W. Weijer, 1999: Indian–Atlantic interocean exchange: Dynamics, estimation and impacts. *J. Geophys. Res.,* **104,** 20 885–20 910.

Döös, K., and A. Coward, 1997: The Southern Ocean as the major upwelling zone of north Atlantic Deep Water. *Int. WOCE Newsl.,* **27,** 3–4.

Fahrbach, E., G. Rohardt, M. Schröder, and V. Strass, 1994: Transport and structure of the Weddell Sea. *Ann. Geophys.,* **12,** 840–855.

Fine, R. A., 1993: Circulation of Antarctic Intermediate Water in the South Indian Ocean. *Deep-Sea Res.,* **40**, 2021–2042.

Fu, L.-L., 1986: Mass, heat, and freshwater fluxes in the South Indian Ocean. *J. Phys. Oceanogr.,* **16,** 1683–1693.

Georgi, D. T., 1979: Modal properties of Antarctic Intermediate Water in the southeast Pacific and South Atlantic. *J. Phys. Oceanogr.,* **9,** 456–468.

——, 1981: On the relationship between the large-scale property variations and fine structure in the Circumpolar Deep Water. *Deep-Sea Res.,* **86,** 6556–6566.

Gordon, A. L., 1986: Interocean exchange of thermocline water. *J. Geophys. Res.,* **91,** 5037–5046.

——, and E. J. Molinelli, 1982: *Southern Ocean Atlas.* Columbia University Press, 11 pp., 233 plates.

——, and B. A. Huber, 1990: Southern Ocean winter mixed layer. *J. Geophys. Res.,* **95,** 11 655–11 672.

——, R. F. Weiss, W. M. Smethie Jr., and M. J. Warner, 1992: Thermocline and intermediate water communication between the South Atlantic and Indian Oceans. *J. Geophys. Res.,* **97,** 7223–7240.

Hellerman, S., and M. Rosenstein, 1983: Normal monthly wind stress over the world ocean with error estimates. *J. Phys. Oceanogr.,* **13,** 1093–1104.

Hogg, N. G., P. Biscaye, W. Gardner, and W. J. Schmitz Jr., 1982: On the transport and modification of Antarctic Bottom Water in the Vema Channel. *J. Mar. Res.,* **40,** 231–263.

Holfort, J., 1994: Großräumige Zirkulation und meridionale Transporte im Südatlantik (in German, English abstract). Ph.D. thesis, Berichte aus dem Institut für Meereskunde an der Christian-Albrechts-Universität Kiel, Nr. 260, 95 pp. [Available from Institute for Marine Research, University of Kiel, Düsternbrooker Weg, 24105 Kiel, Germany.]

Jackett, D., and T. J. McDougall, 1997: A neutral density variable for the world's oceans. *J. Phys. Oceanogr.,* **27,** 237–263.

Keith, D. W., 1995 Meridional energy transports: Uncertainty in zonal means. *Tellus,* **47,** 30–44.

Levitus, S., and T. Boyer, 1994: *World Ocean Atlas 1994.* Vol. 4: *Salinity,* Tech. Rep. NOAA Atlas NESDIS 4, U.S. Department of Commerce, NOAA, NESDIS, 117 pp.

Lutjeharms, J. R. E., and R. C. Van Ballegooyen, 1988: The retroflection of the Agulhas Current. *J. Phys. Oceanogr.,* **18,** 1570–1583.

Macdonald, A. M., 1993: Property fluxes at 30°S and their implication for the Pacific–Indian throughflow and the global heat budget. *J. Geophys. Res.,* **98,** 6851–6868.

——, 1998: The global ocean circulation: A hydrographic estimate and regional analysis. *Progress in Oceanography,* Vol. 41, Pergamon, 281–382.

——, and C. Wunsch, 1996: An estimate of global ocean circulation and heat fluxes. *Nature,* **382,** 436–439.

Marshall, J., D. Jamous, and J. Nilsson, 1999: Reconciling thermodynamic and dynamic methods of computation of water-mass transformation rates. *Deep-Sea Res.,* **46,** 545–572.

McCartney, M. S., 1977: Subantarctic Mode Water. *Deep-Sea Res.,* **24,** 103–119.

——, 1982: The subtropical recirculation of Mode Waters. *J. Mar. Res.,* **40,** 427–464.

McIntosh, P. C., and S. R. Rintoul, 1997: Do box inverse models work? *J. Phys. Oceanogr.,* **27,** 291–208.

Metzl, N., B. Moore, and A. Poisson, 1990: Resolving the intermediate and deep advective flows in the Indian Ocean by using temperature, salinity, oxygen and phosphate data: The interplay of biogeochemical and geophysical tracers. *Geochemical Variability in the Oceans, Ice and Sediments,* L. P. Labeyrie and C. Jeandel, Eds., Vol. 89, *Palaeogeography, Palaeoclimatology, Palaeoecology (Global and Planetary Change Section),* Elsevier Science, 81–111.

Molinelli, E. T., 1981: The Antarctic influence on Antarctic Intermediate Water. *J. Mar. Res.,* **39,** 267–293.

Munk, W. H., 1966: Abyssal recipes. *Deep-Sea Res.,* **13,** 707–730.

Nurser, A. J. G., R. Marsh, and R. G. Williams, 1999: Diagnosing water mass formation from air–sea fluxes and surface mixing. *J. Phys. Oceanogr.,* **29,** 1468–1487.

Orsi, A. H., T. Whitworth III, and W. D. Nowlin Jr., 1995: On the meridional extent and fronts of the Antarctic Circumpolar Current. *Deep-Sea Res.,* **42,** 641–673.

Peterson, R., 1992: The boundary currents in the western Argentine Basin. *Deep-Sea Res.,* **39,** 623–644.

——, and L. Stramma, 1991: Upper-level circulation in the South Atlantic Ocean. *Progress in Oceanography,* Vol. 26, Pergamon, 1–73.

Piola, A. R., and D. T. Georgi, 1982: Circumpolar properties of Antarctic Intermediate Water and Subantarctic Mode Water. *Deep-Sea Res.,* **29,** 687–711.

——, and A. L. Gordon, 1989: Intermediate water in the southwestern South Atlantic. *Deep-Sea Res.,* **36,** 1–16.

Polzin, K. L., and E. Firing, 1997: Estimates of diapycnal mixing using LADCP and CTD data from I8S. *Int. WOCE Newsl.,* **29,** 39–42.

Reid, J. L., 1986: On the total geostrophic circulation of the South

Pacific Ocean: Flow patterns, tracers and transports. *Progress in Oceanography,* Vol. 16, Pergamon, 1–61.

——, 1989: On the total geostrophic circulation of the South Atlantic Ocean: Flow patterns, tracers and transports. *Progress in Oceanography,* Vol. 23, Pergamon, 149–244.

Rintoul, S. R., 1991: South Atlantic interbasin exchange. *J. Geophys. Res.,* **96,** 2675–2692.

——, and J. L. Bullister, 1999: A late winter hydrographic section from Tasmania to Antartica. *Deep-Sea Res.,* **46,** 1417–1454.

Robbins, P. E., and J. M. Toole, 1997: The dissolved silica budget as a constraint on the meridional overturning circulation of the Indian Ocean. *Deep-Sea Res.,* **44,** 879–906.

Sætre, R., and A. J. da Silva, 1984: The circulation of the Mozambique Channel. *Deep-Sea Res.,* **31,** 485–508.

Saunders, P. M., and B. R. King, 1995: Oceanic fluxes on the WOCE A11 Section. *J. Phys. Oceanogr.,* **25,** 1942–1957.

Schmitt, R. W., P. S. Bogden, and C. E. Dorman, 1989: Evaporation minus precipitation and density fluxes for the North Atlantic. *J. Phys. Oceanogr.,* **19,** 1208–1221.

Schmitz, W. J., Jr., 1995: On the interbasin-scale thermohaline circulation. *Rev. Geophys.,* **33,** 151–173.

——, 1996: On the World Ocean Circulation. Vol. II: The Pacific and Indian Oceans/A global update. Tech. Rep. WHOI-96-08, Woods Hole Oceanographic Institute, 237 pp. [Available from Woods Hole Oceanographic Institute, Woods Hole, MA 02543.]

——, and P. L. Richardson, 1991: On the sources of the Florida Current. *Deep-Sea Res.,* **38,** 389–409.

Sloyan, B. M., 1997: The circulation of the Southern Ocean and the adjacent ocean basins determined by inverse methods. Ph.D. thesis, Institute of Antarctic and Southern Ocean Studies, University of Tasmania, 479 pp. [Available from IASOS, University of Tasmania, GPO Box 252-77, Hobart, Tasmania 7001, Australia.]

——, and S. R. Rintoul, 2000: Estimates of area-averaged diapycnal fluxes from basin-scale budgets. *J. Phys. Oceanogr.,* **30,** 2320–2341.

——, and ——, 2001: The Southern Ocean limb of the global deep overturning circulation. *J. Phys. Oceanogr.,* **31,** 143–173.

Speer, K., and E. Tziperman, 1992: Rates of water mass formation in the North Atlantic Ocean. *J. Phys. Oceanogr.,* **22,** 93–104.

——, and W. Zenk, 1993: The flow of Antarctic Bottom Water into the Brazil Basin. *J. Phys. Oceanogr.,* **23,** 2667–2682.

Stommel, H., and A. B. Arons, 1960: On the abyssal circulation of the world's ocean. ii. An idealized model of circulation pattern and amplitude in oceanic basins. *Deep-Sea Res.,* **6,** 140–154.

Stramma, L., 1992: The south Indian Ocean Current. *J. Phys. Oceanogr.,* **22,** 421–430.

——, and R. G. Peterson, 1989: Geostrophic transport in the Benguela Current region. *J. Phys. Oceanogr.,* **19,** 1440–1448.

——, and ——, 1990: The South Atlantic Current. *J. Phys. Oceanogr.,* **20,** 846–859.

——, and J. R. E. Lutjeharms, 1997: The flow field of the subtropical gyre of the South Indian Ocean. *J. Geophys. Res.,* **102,** 5513–5530.

——, R. G. Peterson, and M. Tomczak, 1995: The South Pacific Current. *J. Phys. Oceanogr.,* **25,** 77–91.

Suga, T., and L. D. Talley, 1995: Antarctic Intermediate Water circulation in the tropical and subtropical South Atlantic. *J. Geophys. Res.,* **100,** 13 441–13 453.

Talley, L. D., 1996: Antarctic Intermediate Water in the South Atlantic. *The South Atlantic: Present and Past Circulation,* G. Wefer et al., Eds., Springer, 219–238.

Toggweiler, J. R., and B. Samuels, 1993: New radiocarbon constraints on the upwelling of abyssal water to the ocean's surface. *The Global Carbon Cycle,* M. Heimann, Ed., Vol. 15, *Nato ASI Series I: Global Enviornmental Change,* Springer-Verlag, 333–363.

Toole, J. M., and B. A. Warren, 1993: A hydrographic section across the subtropical South Indian Ocean. *Deep-Sea Res.,* **40,** 1973–2019.

Trèguer, P., D. M. Nelson, A. J. Van Bennekorn, D. J. DeMaster, A. Leynaert, and B. Quèguiner, 1995: The silica balance in the world ocean: A reestimate. *Science,* **268,** 375–379.

Trenberth, K. E., J. Olson, and W. G. Large, 1990: The mean annual cycle in global ocean wind stress. *J. Phys. Oceanogr.,* **20,** 1742–1760.

Tziperman, E., 1986: On the role of interior mixing and air–sea fluxes in determining the stratification and circulation of the oceans. *J. Phys. Oceanogr.,* **16,** 680–693.

——, 1988: Calculating the time-mean oceanic general circulation and mixing coefficient from hydrographic data. *J. Phys. Oceanogr.,* **18,** 519–525.

Walin, G., 1982: On the relation between sea-surface heat flow and thermal circulation in the ocean. *Tellus,* **34,** 187–195.

Warren, B., 1981: Transindian hydrographic section at Lat. 18°S: Property distribution and circulation in the South Indian Ocean. *Deep-Sea Res.,* **28,** 759–788.

Whitworth, T., III, W. D. Nowlin Jr., R. D. Pillsbury, and R. F. Weiss, 1991: Observations of the Antarctic Circumpolar Current and deep boundary current in the Southwest Atlantic. *J. Geophys. Res.,* **96,** 15 105–15 118.

——, B. A. Warren, W. D. Nowlin Jr., S. B. Rutz, R. D. Pillsbury, and M. I. Moore, 1999: On the deep western-boundary current in the Southwest Pacific Basin. *Progress in Oceanography,* Vol. 43, Pergamon, 1–54.

Wijffels, S. E., J. M. Toole, H. L. Bryden, R. A. Fine, W. J. Jenkins, and J. L. Bullister, 1996: The water masses and circulation at 10°N in the Pacific. *Deep-Sea Res.,* **43,** 501–544.

Wunsch, C., 1978: The North Atlantic general circulation west of 50°W determined by inverse methods. *Rev. Geophys. Space Phys.,* **16**(4), 583–620.

——, D. Hu, and B. Grant, 1983: Mass, heat, salt and nutrient fluxes in the South Pacific Ocean. *J. Phys. Oceanogr.,* **13,** 725–753.

Wüst, G., 1935: Die Stratosphäre des Atlantischen Ozeans. *Wissenschaftliche Ergebnisse der Deutschen Atlantischen Expedition auf dem Forschungs und Vermessungsschiff, Meteor 1925–1927.* (*The Stratosphere of the Atlantic Ocean,* W. J. Emery, Ed., Amerind, 1978.)